

Shell helium-burning hot subdwarf B stars as candidates for blue large-amplitude pulsators

H. Xiong,^{1,2,3} L. Casagrande,² X. Chen,^{1,3,4} J. Vos,⁵ X. Zhang,⁶ S. Justham,^{7,8,9,10,11} J. Li,¹³ T. Wu,^{1,3,4,12} Y. Li,^{1,3,4} and Z. Han,^{1,3,4}

¹ Yunnan Observatories, Chinese Academy of Sciences, 396 Yangfangwang, Guandu District, Kunming, 650216, P. R. China

² Research School of Astronomy and Astrophysics, The Australian National University, Canberra, ACT 2611, Australia
e-mail: heran.xiong@anu.edu.au

³ Key Laboratory for the Structure and Evolution of Celestial Objects, Chinese Academy of Sciences, 396 Yangfangwang, Guandu District, Kunming, 650216, P. R. China

⁴ Center for Astronomical Mega-Science, Chinese Academy of Sciences, 20A Datun Road, Chaoyang District, Beijing, 100012, P. R. China

⁵ Astronomical Institute of the Czech Academy of Sciences, CZ-25165, Ondřejov, Czech Republic

⁶ Department of Astronomy, Beijing Normal University, Beijing, 100875, P. R. China

⁷ School of Astronomy & Space Science, University of the Chinese Academy of Sciences, Beijing 100012, China

⁸ The Key Laboratory of Optical Astronomy, National Astronomical Observatories, The Chinese Academy of Sciences, Datun Road, Beijing 100012, China

⁹ University of Chinese Academy of Science, Yuquan Road 19, Shijingshan Block, Beijing 100049, P. R. China

¹⁰ Anton Pannekoek Institute for Astronomy, University of Amsterdam, Science Park 904, 1098XH Amsterdam, The Netherlands

¹¹ Max Planck Institute for Astrophysics, Karl-Schwarzschild-Str. 1, 85748 Garching, Germany

¹² Institute of Theoretical Physics, Shanxi University, Taiyuan 030006, China

¹³ Key Laboratory of Space Astronomy and Technology, National Astronomical Observatories, Chinese Academy of Sciences, Beijing 100101, People's Republic of China

Received September 15, 1996; accepted March 16, 1997

ABSTRACT

Blue large-amplitude pulsators (BLAPs) are a newly discovered type of variable star. Their typical pulsation periods are on the order of a few tens of minutes, with relatively large amplitudes of 0.2–0.4 mag in optical bands, and their rates of period changes are on the order of 10^{-7}yr^{-1} (both positive and negative). They are extremely rare objects and attempts to explain their origins and internal structures have attracted a great deal of attention. Previous studies have proposed that BLAPs may be pre-white dwarfs, with masses around $0.3M_{\odot}$, or core-helium-burning stars in the range of $\sim 0.7–1.1M_{\odot}$. In this work, we use a number of MESA models to compute and explore whether BLAPs could be explained as shell helium-burning subdwarfs type B (SHeB sdBs). The models that best match existing observational constraints have helium core masses in the range of $\sim 0.45–0.5M_{\odot}$. Our model predicts that the positive rate of period change may evolve to negative. The formation channels for SHeB sdBs involve binary evolution and although the vast majority of BLAPs do not appear to be binaries (with the exception of HD 133729), the observational constraints are still very poor. Motivated by these findings, we explored the Roche lobe overflow channel. Of the 304 binary evolution models we computed, about half of them are able to produce SHeB sdBs in long-period binaries that evade detection from the limited observations that are currently available.

Key words. (Stars:) binaries: general – Stars: oscillations (including pulsations) – Stars: peculiar (except chemically peculiar) – (Stars:) subdwarfs

1. Introduction

Pulsating stars are important in astrophysics. For example, through asteroseismology, it is possible to infer the internal structure of pulsating stars and use this information to calibrate some basic parameters of stellar physics (Aerts et al. 2010; Chaplin & Miglio 2013; Bedding et al. 2011; Balona et al. 2011; Huber et al. 2012; Li et al. 2022). Pietrukowicz et al. (2017) discovered a new class of pulsators, with periods of 20 to 40 min and large amplitudes, namely, from 0.2 to 0.4 mags in the optical. By comparison, other pulsators with similar periods, for example, rapidly oscillating Ap stars pulsating in the range of 5 to 24 min have amplitudes from 0.001 to 0.02 mag (e.g., Holdsworth et al. 2018).

Moreover, this new class of pulsators has sawtooth-shaped light curves, similar to those of the fundamental radial mode pulsations of classical Cepheids and RR Lyrae-type stars, and effective temperatures of about 30,000K, similarly to hot subdwarf O/B stars (sdOB), but with much larger luminosities or lower surface gravities that is $\log(g/\text{cm s}^{-2}) < 5.3$. Long-term observations show that the pulsations are very stable and their rates of period change ($r = \dot{P}/P$) are on the order of 10^{-7}yr^{-1} . Pietrukowicz et al. (2017) named these stars "blue large-amplitude pulsators (BLAPs; see for example Córscico et al. 2019, for a succinct review of their properties).

Such stars are extremely rare: among nearly half a million pulsating stars, the OGLE survey (Pietrukowicz et al. 2017; Soszyński et al. 2013, 2014, 2015a,b, 2016; Mróz et al. 2015) found only 14 BLAPs in the Galaxy and none in the Magellanic

System (Pietrukowicz 2018). Ramsay (2018) investigated 10 of the 14 known BLAPs with parallaxes available from Gaia DR2. By dereddening their colors, Ramsay (2018) found that 6 of them had absolute magnitudes and intrinsic colors consistent with the temperature derived from optical spectra in Pietrukowicz et al. (2017) as well as from the theoretical predictions of Byrne & Jeffery (2018), thus confirming their nature as BLAPs. The remaining four were redder and fainter, therefore suggesting that they could have been other types of pulsating variables.

Using Zwicky Transient Facility (ZTF), Kupfer et al. (2019) discovered another class of pulsators, with amplitudes similar to those of BLAPs, but with shorter periods and higher surface gravities and effective temperatures. Therefore, Kupfer et al. (2019) named them high-gravity BLAPs. Moreover, their rarity is comparable that of BLAPs. Recently, McWhirter & Lam (2022) crossmatched Gaia DR2 with the ZTF DR3 and analyzed the period-folded light curves. They identified another 16 BLAPs candidates and six high-gravity BLAPs candidates from over 162 million sources. Many of these candidates actually have pulsation periods longer than the BLAPs originally discovered by Pietrukowicz et al. (2017). Thus, it is likely that the pulsation periods for BLAPs span from a few minutes to almost one hour. Lin et al. (2022) comprehensively studied a peculiar BLAP, TMTS-BLAP-1 aka ZGP-BLAP-01, and gave more detailed physical properties.

In Table 1, we list some parameters for confirmed and candidate BLAPs and high-gravity BLAPs: pulsation period (P), its change rate ($r = \dot{P}/P$), effective temperature (T_{eff}), surface gravity ($\log g$), and helium to hydrogen number ratio ($\log N_{\text{He}}/N_{\text{H}}$). The symbols \checkmark (or $*$) indicates whether absolute magnitudes and intrinsic colors from Ramsay (2018) are consistent (or inconsistent) with the effective temperatures from the literature; the symbols \uparrow (or \odot) denotes confirmed BLAPs (or high-confidence BLAPs). From this table, we see that pulsation periods are in the range of 17 – 60mins (excluding high-gravity BLAPs), that is, significantly larger than those initially discovered. The high-gravity BLAPs have periods in the range of 2 – 8mins. It is worth noticing the apparent existence of a period gap between BLAPs and high-gravity BLAPs.

In the original paper, Pietrukowicz et al. (2017) proposed two possible models accounting for the characteristics of BLAPs that is they are proto low-mass white dwarfs (pre-WD model, $\sim 0.3M_{\odot}$) or core-helium-burning stars with hydrogen-rich inflated envelopes ($\sim 1.0M_{\odot}$, CHeB hot subdwarfs model). Based on the two models, several researchers have tried to reproduce the pulsational properties of BLAPs. Romero et al. (2018) and Córscico et al. (2018) simulated various pre-WD models and provided two possible interpretations for the pulsation modes to account for the pulsation period, that is, the radial fundamental mode and high-order nonradial g modes. However, the rate of period change from radial fundamental mode is higher than observed. The high-order nonradial g modes have comparable rates of period change but are inconsistent with the observation that only a single period is detected in BLAPs. Wu & Li (2018) obtained similar results for the pre-WD model. In their study, pre-WDs with mass around $0.36M_{\odot}$ have properties (effective temperature, surface gravity, and pulsation period from radial fundamental mode) similar to those of BLAPs, except for the rate of period change, that is, $r \sim 10^{-5}\text{yr}^{-1}$, much higher than what has been observed.

Wu & Li (2018) also investigated CHeB hot subdwarf models in detail and found that such stars with masses of $0.7\text{--}1.1M_{\odot}$ are in good agreement with almost all BLAPs properties. Their models have proper surface helium-to-hydrogen number ratios

and rates of period change ($r \sim 10^{-7}\text{yr}^{-1}$) in addition to effective temperatures, surface gravities, and pulsation periods. Based on their study, BLAPs are objects in the middle to late phases of core helium burning stage, with metal-rich models matching r better than metal-poor ones. In their models, however, the H-rich envelope mass is fixed and determined by the total mass. Binary evolution in fact will produce hot subdwarfs with similar total mass but various H-rich envelopes and the evolution properties remarkably depend on the envelope mass (Han et al. 2002, 2003; Heber 2009, 2016; Xiong et al. 2017).

On the other hand, using nonadiabatic analysis with the GYRE stellar oscillation code, Byrne & Jeffery (2020) investigated the pulsation properties of the pre-WD model and the driving mechanism. They showed that, if effects of atomic diffusion and radiative levitation were included, the opacity bump at the iron opacity peak leads to a large instability region, that is, effective temperature from 30 000 K up to 50 000 K at least, $\log g$ from 3 to 7, and the periods of unstable fundamental modes from around 100 seconds up to 2-3 hours. This range encompasses both BLAPs and high-gravity BLAPs. Byrne et al. (2021) then further studied formation channels for BLAPs based on the pre-WD model, using a binary population synthesis method, and showed that both common envelope ejection (CEE) and stable Roche lobe overflow (RLOF) can produce these objects. However, CEE generally produces binaries with short orbital periods. The fact that until recently no companions have been detected for BLAPs (Pietrukowicz et al. 2017; Kupfer et al. 2015; Ramsay 2018; McWhirter et al. 2020) seems inconsistent with this channel. However, one object worthy of attention in Table 1 is HD 133729. Pigulski et al. (2022) reported a BLAP orbiting the main-sequence B-type star HD 133729 on an orbital period of 23.08433 d. The pulsation period of this BLAP is 32.37 min, with an amplitude 0.21 mag and a rate of period change of $-11.5 \times 10^{-7}\text{yr}^{-1}$, which is consistent with that of known BLAPs. The BLAP nature of the companion to HD 133729 was previously missed due to the dilution of the observed amplitude by the brighter primary. The companion of HD 133729 is the only BLAP in a binary system that is presently known, but the discovery of this object suggests that (at least some other) BLAPs might be hidden in binaries which might have been misclassified or missed for various reasons.

Since the origin and structure of BLAPs is still an open question and they have temperatures similar to hot subdwarfs but with inflated envelopes, here we propose that BLAPs are shell-helium-burning (SHeB) hot subdwarfs. In the following, we systematically investigate the observational properties of such models based on a simple asteroseismic analysis and we study the parameter space for producing such objects via binary evolution. Our models are able to aptly replicate existing observations of BLAPs. The paper is organized as follows. First, we describe our construction of certain sdB models, which possess different combinations of H-rich envelope mass and He core mass, and we investigate their period, P , and relative pulsation rate of period change, \dot{P}/P , along the evolutionary tracks. We then analyze how sdBs can form through a RLOF channel in Section 3, along with estimations of their number in the Galaxy and some of the observational signatures of putative companions. We present our conclusions in Section 4.

2. Configuration of BLAPs

Subdwarf B-type stars (hereafter sdBs) are core-helium-burning stars (CHeB) with thin H-rich envelopes, located at the extreme horizontal branch (EHB) of the Hertzsprung Russell diagram

Table 1. List of confirmed and candidate BLAPs and high-gravity BLAPs with some of their parameters from the discovery papers. Symbols \checkmark (*) in the status column denote that their absolute magnitudes and intrinsic colors dereddened by the parallax from Gaia DR2 data are consistent (inconsistent) with the temperatures derived from optical spectra or theoretical predictions (see Ramsay 2018). For BLAPs from Ref (3), the symbols \uparrow denote confirmed status, and \odot denote high-confidence candidates.

Variable	$P(\text{min})$	$\dot{P}/P(10^{-7}\text{yr}^{-1})$	T_{eff}	$\log g$	$\log N_{\text{He}}/N_{\text{H}}$	status	Ref.
OGLE-BLAP-001	28.26	2.90 ± 3.70	30800 ± 500	4.61 ± 0.07	-0.55 ± 0.05	\checkmark	(1)
OGLE-BLAP-002	23.29	-19.23 ± 8.05	-	-	-		(1)
OGLE-BLAP-003	28.46	0.82 ± 0.32	-	-	-	*	(1)
OGLE-BLAP-004	22.36	-5.03 ± 1.57	-	-	-	*	(1)
OGLE-BLAP-005	27.25	0.63 ± 0.26	-	-	-		(1)
OGLE-BLAP-006	38.02	-2.85 ± 0.31	-	-	-	*	(1)
OGLE-BLAP-007	35.18	-2.40 ± 0.51	-	-	-		(1)
OGLE-BLAP-008	34.48	2.11 ± 0.27	-	-	-		(1)
OGLE-BLAP-009	31.94	1.63 ± 0.08	31800 ± 1400	4.40 ± 0.18	-0.41 ± 0.13	\checkmark	(1)
OGLE-BLAP-010	32.13	0.44 ± 0.21	-	-	-	\checkmark	(1)
OGLE-BLAP-011	34.87	6.77 ± 8.87	26200 ± 2900	4.20 ± 0.20	-0.45 ± 0.11	\checkmark	(1)
OGLE-BLAP-012	30.90	0.03 ± 0.15	-	-	-	\checkmark	(1)
OGLE-BLAP-013	39.33	7.65 ± 0.67	-	-	-	*	(1)
OGLE-BLAP-014	33.62	4.82 ± 0.39	30900 ± 2100	4.42 ± 0.26	-0.54 ± 0.16	\checkmark	(1)
high-gravity-BLAP-1	3.34	-	34000 ± 500	5.70 ± 0.05	-		(2)
high-gravity-BLAP-2	6.05	-	31400 ± 600	5.41 ± 0.06	-		(2)
high-gravity-BLAP-3	7.31	-	31600 ± 600	5.33 ± 0.05	-		(2)
high-gravity-BLAP-4	7.92	-	31700 ± 500	5.31 ± 0.05	-		(2)
ZGP-BLAP-01/TMTS-BLAP-1	18.933	22.3 ± 0.9	-	-	-		(3) (5)
ZGP-BLAP-02	48.258	-	-	-	-		(3)
ZGP-BLAP-03	53.705	-	-	-	-		(3)
ZGP-BLAP-04	46.681	-	-	-	-		(3)
ZGP-BLAP-05	54.000	-	-	-	-	\odot	(3)
ZGP-BLAP-06	35.839	-	-	-	-	\odot	(3)
ZGP-BLAP-07	44.627	-	-	-	-	\odot	(3)
ZGP-BLAP-08	35.137	-	-	-	-	\odot	(3)
ZGP-BLAP-09	23.264	-	-	-	-	\uparrow	(3)
ZGP-BLAP-10	55.180	-	-	-	-	\odot	(3)
ZGP-BLAP-11	27.951	-	-	-	-	\odot	(3)
ZGP-BLAP-12	51.619	-	-	-	-		(3)
ZGP-BLAP-13	21.578	-	-	-	-		(3)
ZGP-BLAP-14	17.016	-	-	-	-	\odot	(3)
ZGP-BLAP-15	51.073	-	-	-	-		(3)
ZGP-BLAP-16	37.330	-	-	-	-		(3)
ZGP-HGBLAP-01	2.428	-	-	-	-		(3)
ZGP-HGBLAP-02	6.071	-	-	-	-	\odot	(3)
ZGP-HGBLAP-03	4.203	-	-	-	-	\odot	(3)
ZGP-HGBLAP-04	5.950	-	-	-	-	\odot	(3)
ZGP-HGBLAP-05	8.240	-	-	-	-		(3)
ZGP-HGBLAP-06	6.260	-	-	-	-	\odot	(3)
HD 133729	32.27	-11.5	29000	4.5	-		(4)

(1) Pietrukowicz et al. (2017), (2) Kupfer et al. (2019), (3) McWhirter & Lam (2022), (4) Pigulski et al. (2022), (5) Lin et al. (2022). The \dot{P}/P of OGLE-BLAP-002,-004,-011 are from Wu & Li (2018) and it of ZGP-BLAP-01/TMTS-BLAP-1 is from Lin et al. (2022).

(e.g., Heber 2009, 2016; Geier 2015). The shell helium-burning (SHeB) follows the CHeB phase and we show in this section that some SHeB sdBs may aptly reproduce the properties of BLAPs.

We constructed a certain number of sdB models and study the pulsation periods and their changes along evolutionary tracks. The sdB models are computed with the stellar evolution code named MESA (Modules for Experiments in Stellar Astrophysics, version 15140, see Paxton et al. 2011, 2013, 2015, 2018, 2019). Our study is for Population I stars (i.e., with a metallicity $Z = 0.02$, as in Pietrukowicz et al. 2017). We adopted the nuclear network *pp_cno_extras_o18_ne22.net*, which includes all relevant reactions for H and He burning, and the opacity table

OPAL type II, which allows the abundances of C and O to vary with time. The mixing length parameter, α_{MLT} , is set to 2. For simplicity, no stellar wind or other mass loss mechanism is included in our calculations. The input physics used here is similar to that of previous studies of Population I sdB stars by (Xiong et al. 2017, see also Schindler et al. 2015).

2.1. The sdB model

The main characteristics of sdBs are determined by the helium core mass, M_c , the H-rich envelope mass, M_e , and the element abundances in the envelope. We start by constructing some zero-

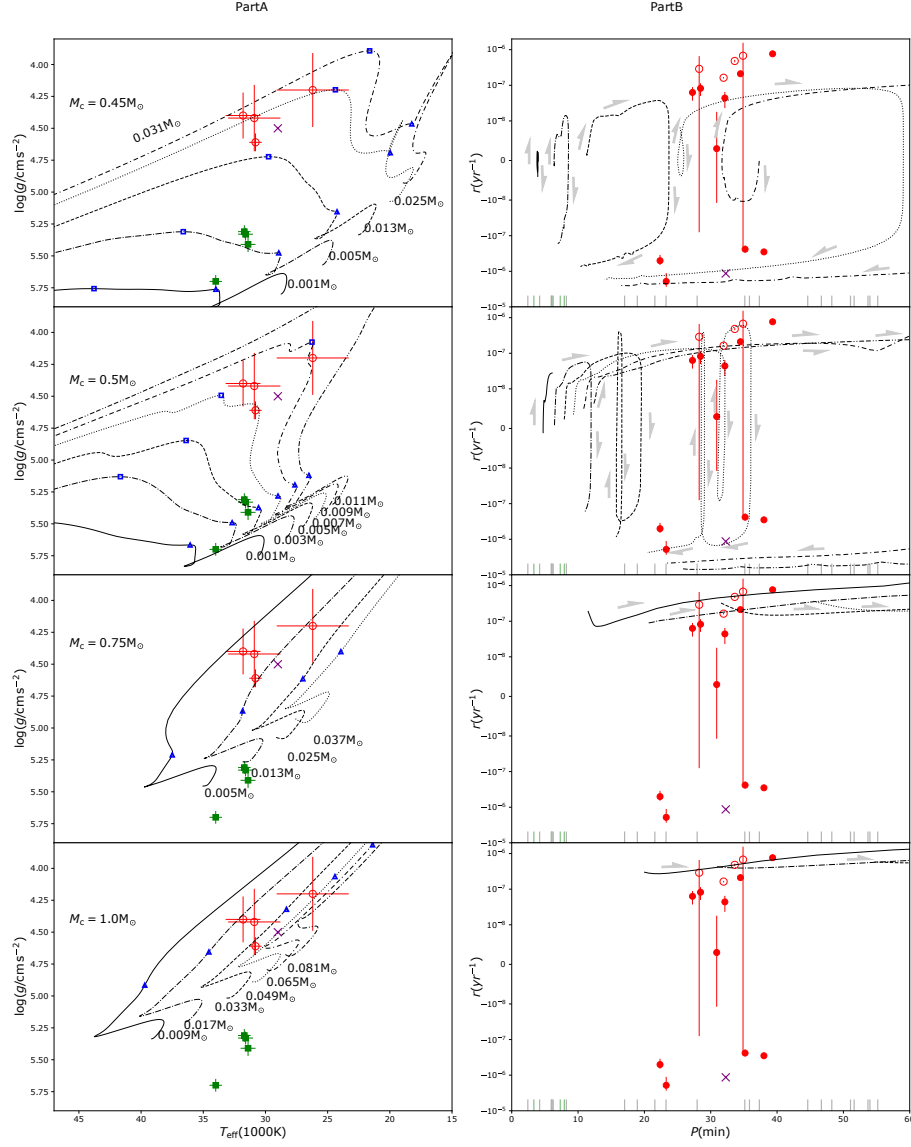


Fig. 1. Evolutionary tracks for constructed sdBs on the ($T_{\text{eff}} - \log g$) diagram (left). In each panel the core mass M_c is reported, along with different values of H-rich envelope mass, M_e , indicated with different linestyles. Four BLAPs (red) and four high-gravity BLAPs (green) with known T_{eff} and $\log g$ are overplotted with error bars for comparison (see Table 1). In the top panel, the loops on the tracks with $M_e = 0.025M_\odot$ and $0.031M_\odot$ are caused by helium core breathing pulses (Li 2012, 2017; Li et al. 2018). To the right, we show the rate of period change $r = \dot{P}/P$ versus pulsation period P for SHeB sdBs, for the same evolutionary tracks of the left panel. The observations of BLAPs (Pietrukowicz et al. 2017, with r), high-gravity BLAPs (Kupfer et al. 2015, without r) and the candidates (McWhirter & Lam 2022, without r) are shown respectively with red dots (open circles highlighting stars with spectroscopic parameters), green ticks (shown as green squares on the left panel), and grey ticks (not shown on the left panel). Purple \times indicates HD 133729 on all panels. There are some markers on both panels to indicate special evolutionary points, and the same markers on the left and right panels are for the same point. Δ indicates the starts of stable SHeB, and \square indicates where are the maximum radius of SHeB phases. So SHeB sdBs evolve from Δ to \square . When the core masses are small (0.45 or $0.5M_\odot$), the SHeB sdBs expand to \square and then shrink to WD ($\Delta \rightarrow \square \rightarrow \text{outside}$); when the core masses are large (0.75 or $1.0M_\odot$), the SHeB sdBs directly expand to giant branch ($\Delta \rightarrow \text{outside}$). The arrows on right panels also indicate the evolutionary direction. We note that the r-axis on Part B applies symlog (symmetrical log) scale, which allows positive and negative values by setting a range around zero within the plot to be linear instead of logarithmic.

age sdBs, that is at the onset of helium burning quietly in the center. We adopt four core masses that is $M_c=0.45, 0.5, 0.75$, and $1.0 M_\odot$, respectively¹. For each core mass, we explore a series of envelope masses starting from an initial value of $M_e = 0.001M_\odot$ and increasing it in steps of $0.002M_\odot$, until the evolutionary

tracks are beyond the region in the $T_{\text{eff}} - \log g$ space where BLAPs are found. In total, we computed more than 80 models, some of which are displayed in Figure 1. In the core, the adopted helium abundance is $Y=0.98$, while the number ratio of helium to hydrogen, $\log N_{\text{He}}/N_{\text{H}}$, in the envelope is set to -0.55 for simplicity. The latter value corresponds to the best atmosphere model fit for OGLE-BLAP-001, which is the prototype object of BLAPs (see Table 1 and Pietrukowicz et al. 2017).

¹ Since we are not interested in the ignition process, nor do we follow the evolution of a star before reaching the sdB phase, in this work we start our analysis from helium-burning quietly in the core.

We then evolved these sdBs to reach the SHeB phase and continue far beyond the location of BLAPs on the Kiel diagram ($T_{\text{eff}} > 50\,000$ K or $\log g < 4.0$). The evolutionary tracks on the $T_{\text{eff}} - \log g$ plane are presented on the left panels of Fig. 1, where the legend indicates the core and envelope mass, and different line-styles mark models with the same envelope mass on the left and right panels. For clarity, not all models are shown in this figure. For comparison, four BLAPs (in red) and four high-gravity BLAPs (in green) with known T_{eff} and $\log g$ are plotted with their error bars (see Table 1), while the purple \times indicates HD 133729. For $M_c = 0.45M_\odot$ (upper panel), we see several loops on the evolutionary tracks when $M_e = 0.025M_\odot$ and $0.031M_\odot$, which are caused by helium core breathing pulses after the exhaustion of the central He (Caloi 1989; Li 2012, 2017; Li et al. 2018; Ostrowski et al. 2021).

2.2. Pulsations and rate of period change, \dot{P}/P

The large amplitude, short periods, and small rates of period change observed in BLAPs still pose a challenge to pulsation theory (Pietrukowicz et al. 2017). A few pioneering asteroseismic investigations have been carried out (for example Romero et al. 2018; Córscico et al. 2018; Wu & Li 2018; Byrne & Jeffery 2020), but none of them can fully explain the existence and the pulsation properties of BLAPs.

In this paper, rather than focusing on a detailed asteroseismic analysis, we explore a new evolutionary pathway to BLAPs. Our goal is thus to compute a broad range of evolutionary models and use these to inform on possible formation channels for BLAPs via binary evolution. While we defer a detailed asteroseismic analysis to a future paper (Wu et al., in prep.), we use the fact that the lightcurves of BLAPs are similar to those of classical pulsators like Cepheid and RR Lyrae-type stars that exhibit just the radial fundamental mode (see for example Córscico et al. 2019, for a discussion of pulsation modes). Thanks to this similarity, we can use simple scaling relations to estimate the pulsation period, P , and rate of period change, $r = \dot{P}/P$, for our models. We describe our method further below.

Confidence in this approach comes from the fact that P and r inferred from scaling relations agree to within 10 percent (5 percent for most BLAPs models) with those computed with detailed asteroseismic analysis via GYRE (Wu et al., in prep). This suffices for the qualitative investigation of Fig. 1. Also, despite our here on SHeB sdB models, we also constructed some $\sim 0.3M_\odot$ pre-WD models; the values of r we derive when these models are located in the BLAPs region of the HR diagram are on the order of 10^{-5} , similar to those obtained by Wu & Li (2018) through detailed asteroseismic analysis.

For p-mode oscillations, we used Eq. (1) to estimate the frequency, ν , with radial order, n , and spherical harmonic degree, l (Tassoul 1980), which is not dependent on the driving mechanism

$$\nu(n, l) \approx (n + l/2 + \epsilon)\Delta\nu, \quad (1)$$

where ϵ is the phase constant ($= 2.625$ according to the best-fitting model in Wu & Li 2018) and $\Delta\nu$ is the large frequency separation, which is defined as the frequency spacing between adjacent radial order mode with the same spherical harmonic degree. The value of $\Delta\nu$ strongly depends on mean density and is estimated by Tassoul (1980)

$$\Delta\nu \approx \Delta\nu_\odot \sqrt{\bar{\rho}/\bar{\rho}_\odot} = \Delta\nu_\odot \sqrt{\frac{M}{M_\odot} \left(\frac{R_\odot}{R}\right)^3}, \quad (2)$$

where $\bar{\rho}$, M , and R are the mean density, mass, and radius of our sdBs models, respectively. $\nu(0, 0) \approx \epsilon\Delta\nu$ is the frequency of fundamental mode, and $\Delta\nu_\odot = 135.1\mu\text{Hz}$ (Huber et al. 2011). The period is the reciprocal of the frequency, $P = 1/\nu(0, 0)$. Then, following the definition of Pietrukowicz et al. (2017) the rate of period change can be estimated as

$$r = \frac{\Delta P}{\Delta t} \frac{1}{P}, \quad (3)$$

which we calculate in this work as:

$$r_n = \frac{P_{n+1} - P_n}{t_{n+1} - t_n} \frac{1}{P_{n+1}}, \quad (4)$$

where n refers to each point along a track computed through MESA. In the right panels of Fig. 1, the rates of period change for our SHeB sdB models are compared to the relative period changes measured by Pietrukowicz et al. (2017) using data from OGLE-III and OGLE-IV: $\dot{P}/P = \frac{\Delta P}{\Delta t} \frac{1}{P_{IV}} = \frac{P_{IV} - P_{III}}{t_{IV} - t_{III}} \frac{1}{P_{IV}}$.

2.3. Results

As shown in Figure 1, SHeB stars have typical rates of pulsation period change, r , on the order of 10^{-7}yr^{-1} , and occasionally on the order of 10^{-6}yr^{-1} . This is comparable to that of observed in confirmed and candidate BLAPs and high-gravity BLAPs. Meanwhile, the values of r may change from positive to negative (and vice versa), due to the fact that P is proportional to the mean density and that P increases or decreases when the star expands or shrinks. For example, for the models with $M_c = 0.45$ and $0.5M_\odot$, r evolves from positive to negative when the stars evolve from expanding to shrinking during their evolution towards the white dwarf sequence. We note that, in most cases, the r value is on the order of 10^{-7}yr^{-1} and the transitions from positive to negative are marked by \square in $T_{\text{eff}} - \log g$ diagrams. The open triangles and open squares in the left panels denote the positions where the transition occurs. The evolution of r may account for the fact that both positive and negative r values have been observed in BLAPs and this can be tested by future monitoring of r . However, the transition is hard to observe, as the sample size of BLAPs is too small.² We do not see such transitions for models with higher core mass $M_c = 0.75$ and $1.0M_\odot$ since these SHeB stars evolve directly to the post-AGB location and will not shrink until the He-rich envelope becomes thin enough. In fact, SHeB stars with $M_c = 0.75$ and $1.0M_\odot$ have pulsation periods larger than observations and cannot cover the locations of high-gravity BLAPs on the $P - r$ plane.

It is worth noticing that the radius fluctuates for models with $M_c = 0.5M_\odot$, resulting in large rates of period change ($r \sim 10^{-6}$) (panels in the second row). The large r could explain BLAPs with positive large values such as OGLE-BLAP-011 and OGLE-BLAP-013. We will investigate this into more detail in a future work. Lin et al. (2022) reported the properties of TMTS-BLAP-1/ZGP-BLAP-01, and it is consistent with SHeB model but disagreed with other models. In this paper, we simply assume that BLAPs and high-gravity BLAPs have the same types of pulsation and we regard the 0.45 and $0.5M_\odot$ models as our high-confidence ones.

² A typical SHeB sdB stays $\sim 2 \times 10^6$ yr in the BLAP region (see Sect 3.3) and if we observe for ten years, the possibility of observing the transition moment is about $10/(2 \times 10^6)$. If we observe for ten years each of the 40 BLAPs, the possibility of observing the transition at least one time is $1 - (1 - (10/(2 \times 10^6)))^{40} \approx 0.02\%$

Figure 1 shows that SHeB models pass through the $T_{\text{eff}} - \log(g)$ region inhabited by BLAPs when the H-rich envelop has the following masses: $M_e = 0.013M_\odot - 0.031M_\odot$ for $M_c = 0.45M_\odot$, $M_e = 0.007M_\odot - 0.011M_\odot$ for $M_c = 0.5M_\odot$, $M_e = 0.005M_\odot - 0.037M_\odot$ for $M_c = 0.75M_\odot$, and $M_e = 0.009M_\odot - 0.081M_\odot$ for $M_c = 1.0M_\odot$. For the high-gravity BLAPs, we obtain $M_e = 0.001M_\odot - 0.013M_\odot$ for $M_c = 0.45M_\odot$, and $M_e = 0.001M_\odot - 0.005M_\odot$ for $M_c = 0.5M_\odot$.

Since our models are able to explain many properties of the BLAPs, in the following discussion, we explore their possible formation channels. An important aspect that will be addressed in future works is to analyze the pulsation stability properties of (some of) our BLAP models. We remark that the study of the excitation and stability of pulsations strongly relies on both microscopic and macroscopic physical processes of elements, such as element diffusion, radiative levitation, and opacity tables (for example Byrne & Jeffery 2018). We plan to analyze pulsation stability across the stellar parameters identified with our models in a future investigation by using non-adiabatic theory and radial stellar pulsation theory to try reproducing light curves and radial velocities observed in BLAPs.

The computation of non-adiabatic pulsations can provide powerful insights into the stability of pulsation modes. For example, in their work on pre-WD models to explain BLAPs, Romero et al. (2018) found the need of super-solar metallicity to drive pulsations via the κ mechanism. The effect of metallicity on the stability of pulsation is particularly interesting, given the lack of BLAPs detected thus far in the metal-poor regime (Pietrukowicz 2018). Since the fraction of close binaries increases at low metallicities (Moe et al. 2019), if our models are not pulsationally unstable at low metallicity, this could have implication for the viability of evolutionary scenarios relying on close period binaries (see the next section).

3. Formation channel(s)

Given the success of our SHeB sdBs models in reproducing a number of BLAPs' properties, in this section we investigate their formation channel(s). Han et al. (2002, 2003) developed a binary model for the formation of sdB stars. This model explained almost all properties of sdB stars, including single sdBs, short- and long-period sdBs³, and thus has been widely accepted in the literature. Our study for BLAPs is based on this model.

Except for HD 133729 (Pigulski et al. 2022), no evidence for companion stars has been found in BLAPs so far (Pietrukowicz et al. 2017; Kupfer et al. 2015; Ramsay 2018; McWhirter et al. 2020). This however does not necessarily imply that BLAPs are single stars. For example, they could be in long-period binaries which have escaped detection or, otherwise, in short-period binaries, where very bright companions dominate the light budget and dilute the pulsation amplitude (similar to HD 133729, see Pigulski et al. 2022). It might also be possible that BLAPs themselves have very faint companions. Radial velocity monitoring might be used to detect binaries, but so far only few BLAPs have spectroscopic observations.

In Han's model, hot subdwarfs can be produced through three channels, namely, CEE, stable RLOF, or a merger of two He WDs (Han et al. 2002, 2003). For the CEE channel, the donor loses most of the H-rich envelope mass close to the tip of RGB during common envelope ejection and the remnant evolves to short-period sdBs. This channel is inconsistent with the -albeit

limited- observations that no BLAP shows sign of being in a short-period binary, except for the case of the companion of HD 133729. Since the CEE process is complicated and is not yet well understood (see Ivanova et al. 2013), it is hard to know the envelope mass of sdBs in this way from binary calculation. However, the locations of observed short-period sdBs in the $T_{\text{eff}} - \log g$ diagram suggest that the H-rich envelopes of sdBs from the CEE channel are massive enough to account for BLAPs (Xiong et al. 2017). If we only consider the envelope mass of sdBs, we cannot exclude the possibility that the CEE produces BLAPs⁴. Therefore, in Section 3.3, we give the expected number of BLAPs also from this channel.

As we have already pointed out, HD 133729 is the only object for which a BLAP has been identified in a binary system and given its parameters it was likely produced via stable RLOF rather than CEE. The (present-day) primary in HD 133729, has a mass of $2.85 \pm 0.25M_\odot$, which means that the donor (which we speculate to have evolved into the BLAP) probably had a mass around $\sim 3.0M_\odot$ (McWhirter & Lam 2022) and non-degenerate core before the RLOF took place. Such a star may become an sdB star (and then a BLAP) if mass transfer starts during the Hertzsprung gap. Based on the work of Han et al. (2003), sdB binaries produced by non-degenerate progenitors via RLOF during a Hertzsprung gap have orbital periods in the range between 10 hours and dozens of days, consistent with the observations of HD 133729.

For the merger channel, two He WDs could merge due to gravitational wave radiation and produce a single hot subdwarf star, with its mass in the range of $0.3 - 0.8M_\odot$ (Han et al. 2002, 2003; Zhang et al. 2009, 2017). During the merger of double He WDs, the less massive He WD is disrupted and accreted onto the more massive one. Helium is ignited through He flashes, and the merged object becomes an sdB star when He burns stably in the center (Zhang & Jeffery 2012). In this case, however, little hydrogen survives the series of He flashes that is the maximum hydrogen mass is only $0.002M_\odot$ in the study of Hall & Jeffery (2016, see also Zhang & Jeffery 2012). This value agrees with the M_e determined for high-gravity BLAPs but it is far less than that required for the other BLAPs ($> 0.005M_\odot$, as discussed in Section 2). Hence, if BLAPs are single sdBs, it is unlikely that they form through the merger of two He WDs⁵.

For the RLOF channel, if the donors have low initial masses ($\lesssim 2M_\odot$) and degenerate He cores after central H burning, the produced hot subdwarfs have masses around $0.5M_\odot$ (Han et al. 2002, 2003) and orbital periods around 1400 days (Chen et al. 2013). If the donors have masses with non-degenerate He cores⁶, the resulting hot subdwarfs have a wide mass range, namely, from $0.3 - 0.8M_\odot$, and the orbital periods are relatively short, namely, from several days to more than one hundred days, depending on the initial mass ratio, initial orbital period, and the assumptions for mass and angular momentum loss (Han et al.

⁴ If sdBs from the CEE channel cannot evolve into the BLAPs, the abundances in the envelope could be the cause since element abundances are crucial for driving the pulsations. There is evidence showing that short-orbital period sdBs resulted from the CEE channel have surface abundances that are significantly different from that of the RLOF (Geier et al. 2022).

⁵ However, we cannot exclude the possibility that BLAPs are single stars according to this. For example, Meng et al. (2020) proposed that BLAPs are possibly the surviving companions of type Ia supernovae with masses of $0.7 - 1.0M_\odot$.

⁶ Although it is typically quoted that non-degenerate cores form beyond $2.0M_\odot$, with the models used in this work this happens for $> 1.99M_\odot$.

³ For the long-period sdBs see Chen et al. (2013); Vos et al. (2019, 2020)

2000; Chen & Han 2002, 2003). In the following, we focus on the RLOF channel with donors ranging from evolved to degenerate He cores and we create long orbital period binaries.

3.1. Binary evolution calculations

Using MESA, we investigate the binary evolution for several binaries consisting of a giant star (the progenitor of sDBs) and an MS or WD companion. The study is based on Population I stars and the basic physics inputs are the same as introduced in Sect. 2. We only evolve donors and consider companions as point sources. In our calculation, the mass transfer rate is calculated by the scheme of Kolb & Ritter (1990), and the mass transfer process is completely non-conservative, that is, all mass lost from the donor onto the MS star is not actually accreted by the MS star, but is lost from the MS and, hence, from the system. The angular momentum lost from the system is then given by the mass loss times the specific angular momentum (i.e., angular momentum per unit mass) of the MS star. No wind loss has been included in the whole evolutionary process. We discuss this point further in Sect. 3.4.

We go on to explore eight values for the initial mass of the giant (the donor: $M_{\text{li}} = 0.79, 0.89, 1.0, 1.12, 1.26, 1.4, 1.58$, and $1.78 M_{\odot}$) and three values for initial giant and MS mass-ratio $q_i = 1.1, 1.25$ and 1.5 . The upper limit of $q_i = 1.5$ here is consistent with the critical mass ratio for dynamically stable mass transfer when the donor is a giant (Han et al. 2002; Chen & Han 2008). For each (M_{li}, q_i) , we increase the initial orbital separation, A_i , in steps of equal ΔA_i , from the minimum separation to produce sDB stars, to the point where the donor cannot fill its Roche lobe on the red giant branch.

3.2. Outcomes from binary evolution

From our binary evolution calculations, we obtain in total 24 sets of long-period SHeB sDBs. For each (M_{li}, q_i) , we obtain some SHeB sDBs passing through the position of BLAPs and that of high-gravity BLAPs. We show an example in Fig. 2, with initial parameters $(M_{\text{li}}, q_i) = (0.79 M_{\odot}, 1.5)$: the upper panel displays evolutionary tracks in the $T_{\text{eff}} - \log g$ plane, while the lower one shows those in the $P - r$ diagram. A total of 11 evolutionary tracks (including 5 tracks overlapping in the thick gray line) are shown in Fig. 2, with initial orbital periods (\sim orbital periods before RLOF) equally spaced in terms of log. When the initial orbital periods are short, the produced sDBs nearly have no H-rich envelope due to delayed He flashes (Xiong et al. 2017) and the evolutionary tracks are overlapped, as shown with thick grey line in the upper panel.

As shown in the upper of Fig. 2, several SHeB sDBs with relatively high envelope mass match the location of BLAPs, while some with relatively low envelope mass match the location of high-gravity BLAPs, similarly to what has already been shown in Fig. 1. The pulsation period and its rate of change match the observations in terms of the right order of magnitude. All models have orbital period of ~ 1400 days and the companion is a $0.53 M_{\odot}$ main sequence star due to no accretion in the RLOF process (mass transfer is completely nonconservative).

The results for the other explored sets of (M_{li}, q_i) are qualitatively similar to those shown here, (presented in Figs. A1-A23 in the appendix). All sDBs we produce have very similar evolutionary tracks in both the $T_{\text{eff}} - \log g$ and $P - r$ diagrams. They also have orbital periods greater than 1000 days, with companions in the mass range of $0.53 - 1.62 M_{\odot}$.

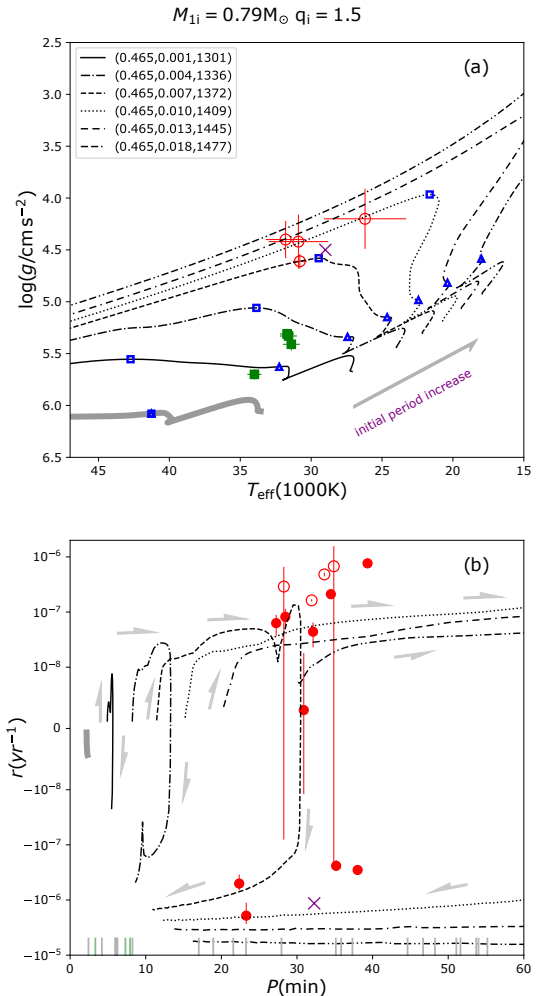


Fig. 2. Evolution of sDBs produced via binary evolution for $(M_{\text{li}}, q_i) = (0.79 M_{\odot}, 1.5)$. The thick gray line identifies overlapping evolutionary tracks (there are five tracks overlapping in this figure, see text for details). Panel (a): Evolutionary tracks in the $T_{\text{eff}} - \log g$ plane. Each linestyle corresponds to a different set of $(M_c, M_e, P_{\text{orb}})$ at the start of stable CHeB (see legend). Panel (b): Rate of period change, r , versus pulsation period, P , for the models in panel (a). The final orbital periods for these models are ~ 1400 days. Observations are the same as in Fig. 1.

We remark that it is somewhat difficult for our models to explain the relatively high positive r values observed in some BLAPs; however, we can clearly see in Fig. 1 that some models may reproduce it. This happens more easily for high He-core masses $M_c = 0.75 M_{\odot}$ and $1.00 M_{\odot}$, and even for $M_c = 0.5 M_{\odot}$ when fine-tuning envelope masses. This seems to suggest that RLOFs with non-degenerate donors might also be a viable channel for BLAP formation and they are worthy of more investigations in a future work.

3.3. Number of BLAPs in the Galaxy

According to our calculation, about 25 to 50 percent (marked with r_1) of sDBs would evolve to become BLAPs during their lives⁷. Considering that the typical lifetime of sDBs is $t_{\text{sDB}} \sim$

⁷ We have computed a total of 304 evolution tracks and between ~ 80 and ~ 160 pass through the location of BLAPs. This range is due to the

10^8 yrs and the lifetime of SHeB sdBs is $t_{\text{shell}} \sim 5 \times 10^7$ yrs, we can simply estimate the number of SHeB sdBs produced in this way as $N_{\text{shell}} = r_1 * N_{\text{sdb}} * t_{\text{shell}} / t_{\text{sdb}}$, where N_{sdb} is the number of sdBs produced from the RLOF channel in the Galaxy.

From the study of Han et al. (2003), $N_{\text{sdb}} = 4.36 \times 10^6$. We therefore have $N_{\text{shell}} \sim 0.5 - 1 \times 10^6$. The number of BLAPs depends on the parameter space defined for BLAPs. A typical SHeB sdB stays $\sim 2 \times 10^6$ yrs in the BLAP region defined by Pietrukowicz et al. (2017), only about 1/20 (marked with r_2) of the SHeB sdB time. Also, not all stars in the instability region show pulsations. For example, ten percent of subdwarfs in the rapid variability region (sdBVr, Østensen et al. 2010) and 75 percent in the slow variability region (sdBVs, Green et al. 2003) show pulsations. We hence assume the fraction of stars showing pulsation to be in the range $r_3 = 0.1 - 1$. The number of BLAPs produced through the RLOF channel therefore can be estimated as $N_{\text{BLAPs}} = r_2 * r_3 * N_{\text{shell}}$, ranging from ~ 2500 to ~ 50000 .

Observationally, we can estimate the number of BLAPs from existing data. For example, McWhirter & Lam (2022) discovered 22 BLAPs candidates (six of which are high-gravity ones) by cross-matching Gaia DR2 and ZTF DR3 using a sample of over 162 million sources satisfying a number of photometric and astrometric cuts. Excluding for simplicity the impact of these cuts on sample selection, a plain scaling to the number of stars in the Milky Way (which is in the range 100-400 billion stars), gives an estimated number of BLAPs candidates between 10^4 and 10^5 . If half of them are BLAPs, their number should be of a few tens of thousands, which finely matches our estimates obtained from SHeB sdBs formed through RLOF channel, although uncertainties are still admittedly large. Our estimates are also consistent with the range 280 to 28000 derived by Meng et al. (2020) from the OGLE survey under the two extreme assumptions that all BLAPs had been discovered, or that 99 percent of them had been missed, respectively.

If we consider that the CEE channel may also contribute to the formation of BLAPs, and assume sdBs from CEE have an envelope mass as similar to that from RLOF, from the study of Han et al. (2003), we have $N_{\text{sdb}} = 6.18 \times 10^6$ for both the CEE+RLOF channels. Keeping the other assumptions unchanged, the estimated N_{BLAPs} ranges from ~ 3500 to ~ 70000 , still consistent with the observations. In further work, a detailed stellar population synthesis (like Byrne et al. 2021, and Alexey et al. in preparation) may give a more precise number and the distribution of properties of BLAPs.

3.4. Putative BLAPs companions

In our calculations, all SHeB sdBs likely to be observed as BLAPs have relatively long orbital periods, $P \sim 1400$ days. The companions are main-sequence stars with lower mass limit, since the mass transfer is set to be completely non-conservative and the companion will not accrete any material during the RLOF. In this section, we explore and quantify the impact of such companions on photometry and radial velocities.

In Fig. 3, we show the spectral energy distribution (SED) of a star with BLAP-like stellar parameters, in comparison to typical A- to M-type main sequence stars. We use synthetic fluxes at solar metallicity from the grid of Castelli & Kurucz (2003), rescaled by the square of the adopted stellar radius and interpolated at the appropriate T_{eff} and $\log g$ (see Table 2 for the adopted

Table 2. Physical parameters adopted for the SED of main sequence stars orbiting a BLAP. For the latter, we adopted the values from one of our binary models. For main sequence companions, we used literature parameters for an archetypal spectral types (Zombeck 2007).

Spec. type	T_{eff} (K)	$\log g$	$R(R_{\odot})$	$M(M_{\odot})$	archetypal
BLAP	27718	4.51	0.62	0.469	
A0	10800	4.15	2.50	3.20	α CrB A
F0	7240	4.44	1.30	1.70	γ Vir
G0	5920	4.44	1.05	1.10	β Com
K0	5240	4.47	0.85	0.78	70 Oph A
M0	3800	4.80	0.51	0.60	Lacaille 8760

values). All stars are assumed to be at the same distance. For comparison, we also plot a number of filter transmission curves from the ultraviolet to the mid-infrared. From panel (a1) we can clearly see that for most spectral types the flux of the BLAP is dominant over the main-sequence companion. Sufficiently hot main sequence stars, however, can become dominant in the optical (A-type) or in the infrared (F-type), depending on the adopted radii. Panel (a2) shows similar comparison, but this time for the monochromatic magnitude difference between the flux of the main-sequence companion and that of the BLAP.

Observationally, however, this hypothetical binary systems must have been unresolved so far. This means that only the total flux can be observed. To account for this, in panel (b1) we compare the flux of a single BLAP (red) against that of a BLAP with a companion. The slope of the SED in the ultraviolet is largely determined by the T_{eff} of the BLAP, but it is altered by the flux of a companion at increasingly longer wavelengths. This excess amounts to ~ 0.1 mag for an M companion in the mid-infrared and it is considerably larger for earlier spectral types. However, it must be kept in mind that the effective temperature and the radius of a BLAP might vary quite considerably while pulsating, thus complicating the detectability of potential companions.

Now let us consider the possibility of looking for binarity through radial velocity variations. From our models, a BLAP with mass $0.458 M_{\odot}$ orbiting a companion of $1.62 M_{\odot}$ on a period of 1366 days will have an orbital speed of 19 km/s, assuming circular orbit. A model with a significantly less massive primary on similar period (0.465, 0.72, 1372) has an orbital speed of 11 km/s. These values will decrease with the inclination angle at which the system is observed. If BLAPs are instead composed of binaries with short periods, the radial velocity signal will be significantly higher. It is thus reasonable to aim for a radial velocity precision on the order of one km/s to test whether BLAPs have companions.

To explore this possibility in more detail, we simulated the radial velocity precision that can be achieved with spectra of various resolution (R) and signal-to-noise ratio (S/N). For the sake of simplicity, we fixed the parameters of the BLAP at $T_{\text{eff}} = 30,000$ K, $\log g = 4.5$ dex, and solar metallicity using a TLUSTY synthetic spectrum (Lanz & Hubeny 2003). We generated 100 spectra in the wavelength range 3800 – 7400 Å for several values of resolution and signal-to-noise, and then estimated the radial velocity precision by computing the standard deviations of the radial velocities that are measured via cross-correlation function (Tonry & Davis 1979). As shown in Fig. 4, radial velocity errors decrease with increasing spectral resolution and signal-to-noise, achieving a km/s precision when $R > 4000$ and $S/N > 25$. It should, however, be pointed out that our results are idealized as they do not include uncertainties arising from instrumental effects, nor the contribution from the pulsations of

uncertainty on the location of BLAPs in the $T_{\text{eff}} - \log g$ diagram. For example, the first 14 BLAPs discovered by Pietrukowicz et al. (2017) cover a much smaller region than that reported in the most recent works.

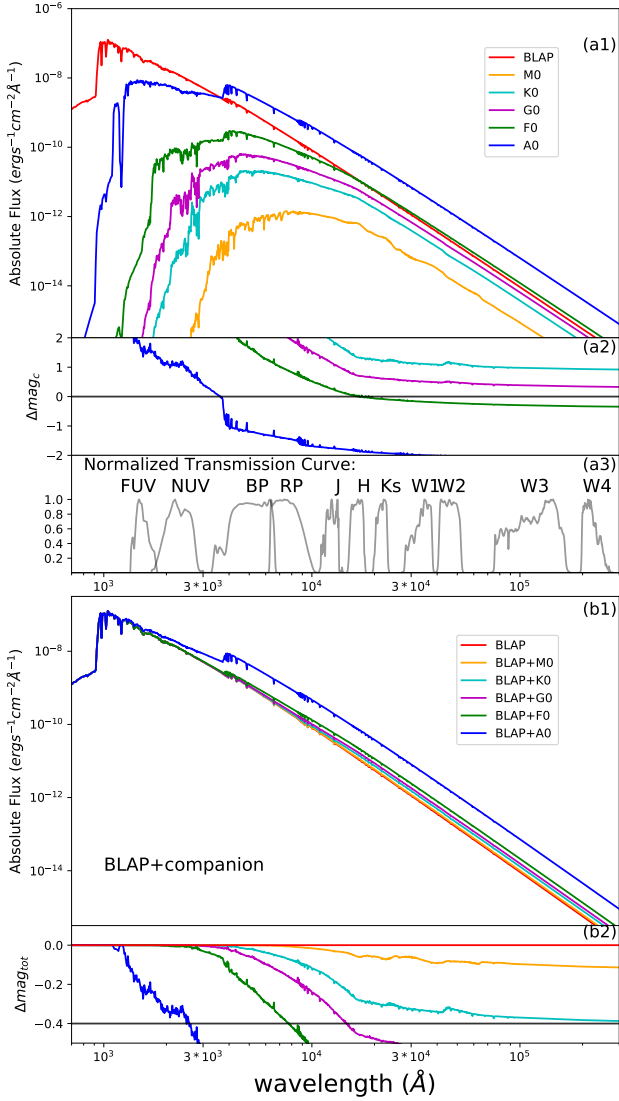


Fig. 3. The expected differences in SED between a BLAP have a companion or not. Panel *a1* (*b1*): Individual (combined) spectral energy distributions for the BLAP and main sequence companions listed in Table 2. Panel *a2* and *b2*: Monochromatic magnitude differences. See text for details. The filters transmission curves are *FUV* and *NUV* from GALEX, *BP* and *RP* from Gaia, *J*, *H*, and *K_s* from 2MASS and *W1*, *W2*, *W3*, and *W4* from WISE.

a BLAP. These would dominate the radial velocity error when integrating over a pulsation period, although stable radial velocity monitoring over a long period of time would still be able to detect the modulation due to a companion over the short period pulsations.

3.5. Discussion

Our study assumes that the mass transfer processes in this part of parameter space are completely nonconservative, namely, that all the mass lost from the giant is lost from the system. If the mass transfer is somehow conservative, the results of RLOF will change. Also, different assumptions for mass and angular momentum loss will result in different parameter spaces for producing sdB stars that is, the range of A_1 for a given M_{1i} and q_i .

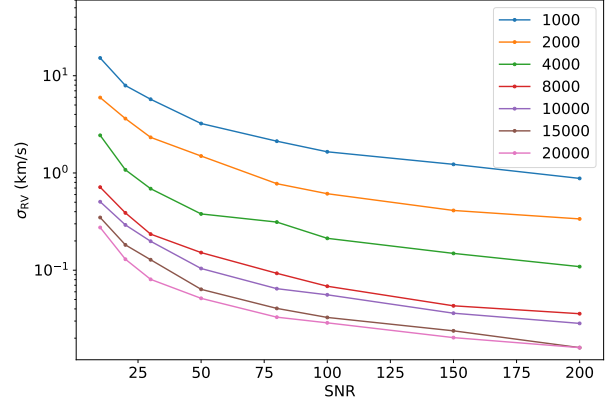


Fig. 4. Errors (standard deviations) of the radial velocities measured by using the method of cross-correlation function for different spectrum resolution (R) and S/N . Colors indicate the resolution.

However, as donors in our study have degenerate cores, the results satisfy a unique sdB mass - orbital period relation (Chen et al. 2013). This means that the orbital period will not change if the sdB mass stays constant, and only the mass of the companion changes. Therefore, the sdB binaries formed through RLOF channel have the same characteristics of our results (i.e., core mass, envelope mass, and orbital period), although the companion would become more massive than that given in this study and may become a blue straggler (see Chen & Han 2008). And a more massive companion would be easier to be detected via SED and the BLAP would have a higher radial velocity (as described in Sect. 3.4).

We have not considered the case where the companion is a WD in our model. We explain this as follows. To ensure the mass transfer process is dynamically stable, the pre-mass-transfer mass of the giant is very restricted, that is, the mass ratio of the giant to the WD is expected to be below a value of $\sim 1.1 - 1.3$ (see table 3 of Han et al. 2002). This generally requires very massive WD companions. Since massive WDs are very rare, they are unlikely to be the companions of BLAPs. In fact, Han et al. (2003) have not obtained any sdB stars with a WD companion in their model. However, based on an adiabatic mass loss model, Ge et al. (2013, 2015) obtained significantly larger critical mass ratios for the stability of mass transfer when the donor is on the giant branch, indicating that the WD mass could be lower than believed for stable mass transfer. We estimated the impact of the critical mass ratios and obtained a few sdB+WD binaries from the RLOF channel indeed based on the criterion of the Ge et al. (2020). But the number is very small and the WD companions to BLAPs should consequently be very rare. For the case of neutron star (NS) or black hole companions, the mass transfer is more likely to be stable due to massive companions. According to the study of Wu et al. (2019), one percent of sdBs have NS companions with long periods (~ 1000 days), we thus may expect $\sim 20 - 500$ BLAPs with NS companions – in a similar way to what is explained in Section 3.3.

The CEE channel will generate sdBs in short period binaries. However, it is still an open question how much H-rich envelope will be left after the CEE (Xiong et al. 2017), due to the huge uncertainties in common envelope evolution (see Ivanova et al. 2013). Presently we cannot rule out the possibility that some sdBs from CEE have relatively thick H-rich envelopes and

show characteristics similar to BLAPs. Their companions could be discovered from radial-velocity variations (see footnote 8). HD 133729 proves that BLAPs in short-period binary do exist, implying that the CEE channel might be a viable formation scenario. Because the primary is a B-type main sequence with $\sim 2.5M_{\odot}$, the progenitor of this BLAP would be an intermediate mass star, which is outside of our grid. According to Han et al. (2003), HD 133729 also could be produced by the RLOF channel, in which the RLOF occurs on Hertzsprung gap. We will investigate this possibility in future work.

4. Conclusions

In this paper, we explore whether SHeB sDBs can reproduce the properties of BLAPs and we discuss their formation channels, based on binary evolution. Our study has shown that some SHeB sDBs aptly reproduce the properties of BLAPs, namely, effective temperature, surface gravity (or luminosity), and the rate of period change. Given that the purpose of this paper is to explore a new evolutionary pathway to BLAPs and narrow down its parameter space, we made use of simple scaling relations to infer the pulsation period and rate of period change for our models. The best-fitting sDB models are in the mass range $0.45 - 0.5M_{\odot}$, which can explain both BLAPs and high-gravity BLAPs. On the contrary, models with higher masses ($0.75 - 1.0M_{\odot}$) are not able to reproduce the properties of high-gravity BLAPs. A prediction of our modeling is that positive r values may change into negative ones.

We performed a series of binary evolution calculations to investigate the formation of BLAPs through the RLOF channel. From our grid of 304 models, we have found that 142 SHeB sDBs could be good BLAP candidates. All these BLAP candidates have long orbital periods, that is, ≥ 1400 days. Because of these periods and the faintness of known BLAPs, the detection of companions would require dedicated radial velocity monitoring. Main sequence companions might also be detected through their flux excess when carrying out the SED fitting.

We also briefly discuss how CEE and the double He WDs merger scenarios might produce sDBs with characteristics similar to BLAPs. The CEE channel preferentially leads to short-period binaries, which would be easier to detect than long-period ones through radial velocity monitoring. Since the fraction of close binaries increases at low metallicity (Moe et al. 2019), pulsation stability in the metal poor regime might give important constraints on the suitability of such a scenario. The merger of double He WDs leads instead to the formation of single sDBs with very thin hydrogen envelopes – far less than required for BLAPs, but consistent with high-gravity BLAPs. We thus conclude that dedicated radial velocity monitoring of BLAPs could help to unveil the origin of these mysterious objects.

Acknowledgements

The authors gratefully acknowledge insightful comments by P. Pietrukowicz, which helped to improve the paper. We thank the anonymous referee for their comments which have helped to improve the paper. This work is partially supported by the Natural Science Foundation of China (Grant no. 11733008, 12125303, 12090040/3), the China Manned Space Project of No. CMS-CSST-2021-A10. J. Vos acknowledges support from the Grant Agency of the Czech Republic (GAČR 22-34467S). The Astronomical Institute Ondřejov is supported by the project RVO:67985815. S. Justham acknowledges funding from the

Netherlands Organisation for Scientific Research (NWO), as part of the Vidi research program BinWaves (project number 639.042.728, PI: de Mink). T. Wu thanks the supports from the B-type Strategic Priority Program of the Chinese Academy of Sciences (Grant No. XDB41000000), from the National Key R&D Program of China (Grant No. 2021YFA1600402), from the NSFC of China (Grant Nos. 11873084, 12133011, and 12273104), from Youth Innovation Promotion Association of Chinese Academy of Sciences, and from Ten Thousand Talents Program of Yunnan for Top-notch Young Talents.

References

- Aerts, C., Christensen-Dalsgaard, J., & Kurtz, D. W. 2010, *Asteroseismology*
- Balona, L. A., Pigulski, A., De Cat, P., et al. 2011, *MNRAS*, 413, 2403
- Bedding, T. R., Mosser, B., Huber, D., et al. 2011, *Nature*, 471, 608
- Byrne, C. M. & Jeffery, C. S. 2018, *MNRAS*, 481, 3810
- Byrne, C. M. & Jeffery, C. S. 2020, *MNRAS*, 492, 232
- Byrne, C. M., Stanway, E. R., & Eldridge, J. J. 2021, *MNRAS*, 507, 621
- Caloi, V. 1989, *A&A*, 221, 27
- Castelli, F. & Kurucz, R. L. 2003, in *Modelling of Stellar Atmospheres*, ed. N. Piskunov, W. W. Weiss, & D. F. Gray, Vol. 210, A20
- Chaplin, W. J. & Miglio, A. 2013, *ARA&A*, 51, 353
- Chen, X. & Han, Z. 2002, *MNRAS*, 335, 948
- Chen, X. & Han, Z. 2003, *MNRAS*, 341, 662
- Chen, X. & Han, Z. 2008, *MNRAS*, 387, 1416
- Chen, X., Han, Z., Deca, J., & Podsiadlowski, P. 2013, *MNRAS*, 434, 186
- Córsico, A. H., Althaus, L. G., Miller Bertolami, M. M., & Kepler, S. O. 2019, *A&A Rev.*, 27, 7
- Córsico, A. H., Romero, A. D., Althaus, L. G., Pelisoli, I., & Kepler, S. O. 2018, *arXiv e-prints*, arXiv:1809.07451
- Ge, H., Webbink, R. F., Chen, X., & Han, Z. 2013, in *IAU Symposium*, Vol. 290, *Feeding Compact Objects: Accretion on All Scales*, ed. C. M. Zhang, T. Belloni, M. Méndez, & S. N. Zhang, 213–214
- Ge, H., Webbink, R. F., Chen, X., & Han, Z. 2015, *ApJ*, 812, 40
- Geier, S. 2015, *Astronomische Nachrichten*, 336, 437
- Geier, S., Dorsch, M., Pelisoli, I., et al. 2022, *A&A*, 661, A113
- Green, E. M., Fontaine, G., Reed, M. D., et al. 2003, *ApJ*, 583, L31
- Hall, P. D. & Jeffery, C. S. 2016, *MNRAS*, 463, 2756
- Han, Z., Podsiadlowski, P., Maxted, P. F. L., & Marsh, T. R. 2003, *MNRAS*, 341, 669
- Han, Z., Podsiadlowski, P., Maxted, P. F. L., Marsh, T. R., & Ivanova, N. 2002, *MNRAS*, 336, 449
- Han, Z., Tout, C. A., & Eggleton, P. P. 2000, *MNRAS*, 319, 215
- Heber, U. 2009, *ARA&A*, 47, 211
- Heber, U. 2016, *PASP*, 128, 082001
- Holdsworth, D. L., Saio, H., Bowman, D. M., et al. 2018, *MNRAS*, 476, 601
- Huber, D., Bedding, T. R., Stello, D., et al. 2011, *ApJ*, 743, 143
- Huber, D., Ireland, M. J., Bedding, T. R., et al. 2012, *ApJ*, 760, 32
- Ivanova, N., Justham, S., Chen, X., et al. 2013, *A&A Rev.*, 21, 59
- Kolb, U. & Ritter, H. 1990, *A&A*, 236, 385
- Kupfer, T., Bauer, E. B., Burdge, K. B., et al. 2019, *ApJ*, 878, L35
- Kupfer, T., Geier, S., Heber, U., et al. 2015, *VizieR Online Data Catalog*, 357
- Lanz, T. & Hubeny, I. 2003, *ApJS*, 146, 417
- Li, Y. 2012, *ApJ*, 756, 37
- Li, Y. 2017, *ApJ*, 841, 10
- Li, Y., Bedding, T. R., Murphy, S. J., et al. 2022, *Nature Astronomy* [arXiv:2204.06203]
- Li, Y., Chen, X.-h., Xiong, H.-r., et al. 2018, *ApJ*, 863, 12
- Lin, J., Wu, C., Wang, X., et al. 2022, *arXiv e-prints*, arXiv:2209.06617
- McWhirter, P. R. & Lam, M. C. 2022, *MNRAS* [arXiv:2201.11862]
- McWhirter, P. R., Lam, M. C., & Steele, I. A. 2020, *MNRAS*, 496, 1105
- Meng, X.-C., Han, Z.-W., Podsiadlowski, P., & Li, J. 2020, *ApJ*, 903, 100
- Moe, M., Kratter, K. M., & Badenes, C. 2019, *ApJ*, 875, 61
- Mróz, P., Udalski, A., Poleski, R., et al. 2015, *Acta Astron.*, 65, 313
- Østensen, R. H., Oreiro, R., Solheim, J. E., et al. 2010, *A&A*, 513, A6
- Ostrowski, J., Baran, A. S., Sanjayan, S., & Sahoo, S. K. 2021, *MNRAS*, 503, 4646
- Paxton, B., Bildsten, L., Dotter, A., et al. 2011, *ApJS*, 192, 3
- Paxton, B., Cantiello, M., Arras, P., et al. 2013, *ApJS*, 208, 4
- Paxton, B., Marchant, P., Schwab, J., et al. 2015, *ApJS*, 220, 15
- Paxton, B., Schwab, J., Bauer, E. B., et al. 2018, *ApJS*, 234, 34
- Paxton, B., Smolec, R., Schwab, J., et al. 2019, *ApJS*, 243, 10
- Pietrukowicz, P. 2018, in *The RR Lyrae 2017 Conference. Revival of the Classical Pulsators: from Galactic Structure to Stellar Interior Diagnostics*, ed. R. Smolec, K. Kinemuchi, & R. I. Anderson, Vol. 6, 258–262

- Pietrukowicz, P., Dziembowski, W. A., Latour, M., et al. 2017, *Nature Astronomy*, 1, 0166
- Pigulski, A., Kotysz, K., & Kolaczek-Szymanski, P. A. 2022, *arXiv e-prints*, arXiv:2203.11789
- Ramsay, G. 2018, *A&A*, 620, L9
- Romero, A. D., Córscico, A. H., Althaus, L. G., Pelisoli, I., & Kepler, S. O. 2018, *MNRAS*, 477, L30
- Schindler, J.-T., Green, E. M., & Arnett, W. D. 2015, *ApJ*, 806, 178
- Soszyński, I., Pawlak, M., Pietrukowicz, P., et al. 2016, *Acta Astron.*, 66, 405
- Soszyński, I., Stepień, K., Pilecki, B., et al. 2015a, *Acta Astron.*, 65, 39
- Soszyński, I., Udalski, A., Szymański, M. K., et al. 2013, *Acta Astron.*, 63, 21
- Soszyński, I., Udalski, A., Szymański, M. K., et al. 2014, *Acta Astron.*, 64, 177
- Soszyński, I., Udalski, A., Szymański, M. K., et al. 2015b, *Acta Astron.*, 65, 297
- Tassoul, M. 1980, *ApJS*, 43, 469
- Tonry, J. & Davis, M. 1979, *AJ*, 84, 1511
- Vos, J., Bobrick, A., & Vučković, M. 2020, *A&A*, 641, A163
- Vos, J., Vučković, M., Chen, X., et al. 2019, *MNRAS*, 482, 4592
- Wu, T. & Li, Y. 2018, *MNRAS*, 478, 3871
- Wu, Y., Chen, X., Chen, H., Li, Z., & Han, Z. 2019, *arXiv e-prints*, arXiv:1912.07705
- Xiong, H., Chen, X., Podsiadlowski, P., Li, Y., & Han, Z. 2017, *A&A*, 599, A54
- Zhang, X., Chen, X., & Han, Z. 2009, *A&A*, 504, L13
- Zhang, X., Hall, P. D., Jeffery, C. S., & Bi, S. 2017, *ApJ*, 835, 242
- Zhang, X. & Jeffery, C. S. 2012, *MNRAS*, 419, 452
- Zombeck, M. 2007, *Handbook of Space Astronomy and Astrophysics: Third Edition*

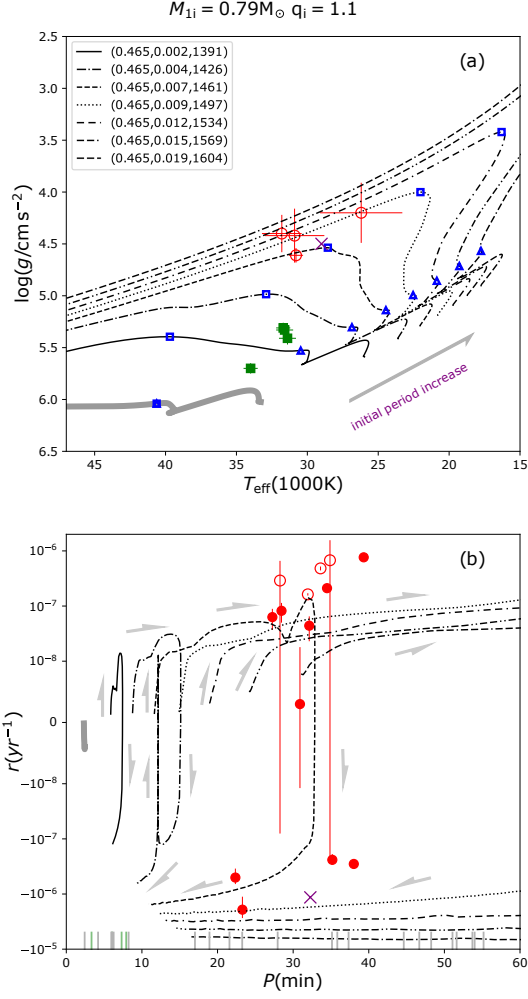


Fig. A.1. Evolution of sdBs produced by binaries, which is same as in Fig. 1, but for $(M_{1i}, q_i) = (0.79 M_{\odot}, 1.1)$.

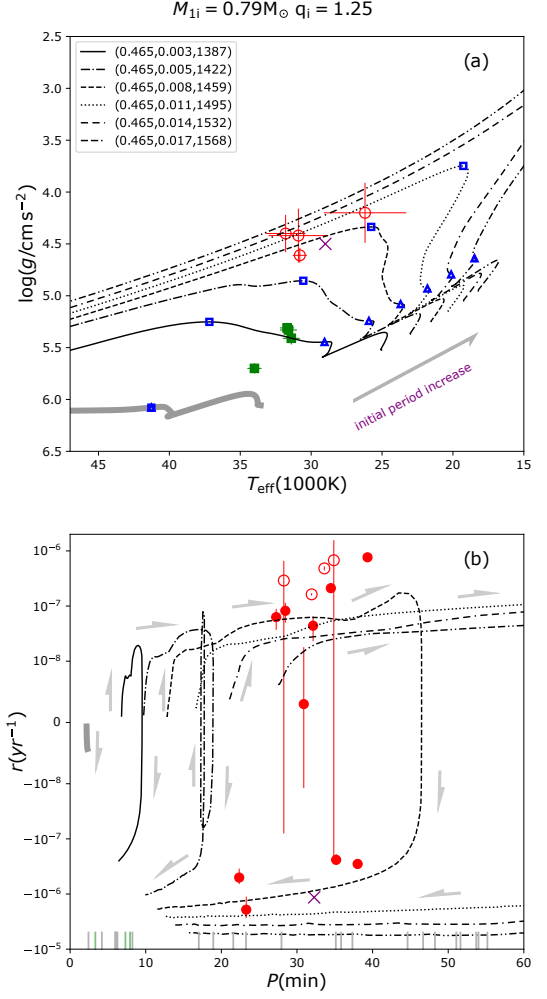


Fig. A.2. Evolution of sdBs produced by binaries, which is same as in Fig. 1, but for $(M_{1i}, q_i) = (0.79 M_{\odot}, 1.25)$.

Appendix A: $T_{\text{eff}} - \log g$ and $P - r$ diagram of SHeB SdBs produced by RLOF channel

The evolutionary tracks on $T_{\text{eff}} - \log g$ and $P - r$ diagrams from binary evolution (see Sect. 3.2). In Sect. 3.2, we only display the results for one (M_{1i}, q_i) , here, we show other results.

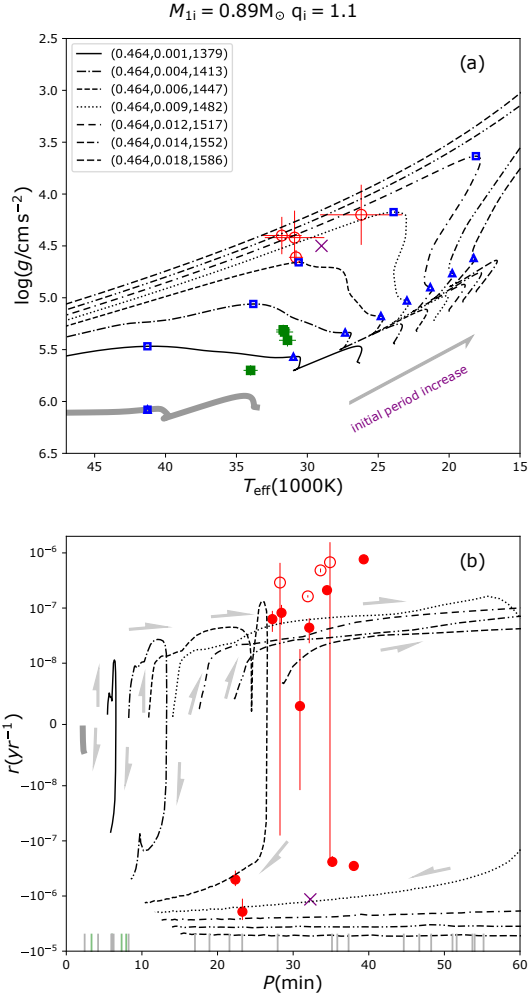


Fig. A.3. The evolution of sdBs produced by binaries, which is same as in Fig. 1, but for $(M_{1i}, q_i) = (0.89M_{\odot}, 1.1)$.

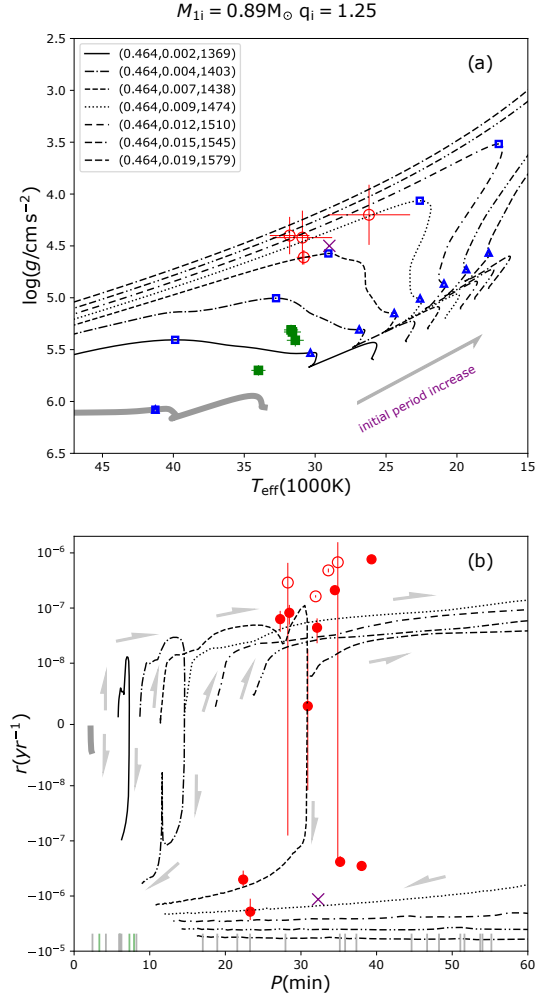


Fig. A.4. The evolution of sdBs produced by binaries, which is same as in Fig. 1, but for $(M_{1i}, q_i) = (0.89M_{\odot}, 1.25)$.

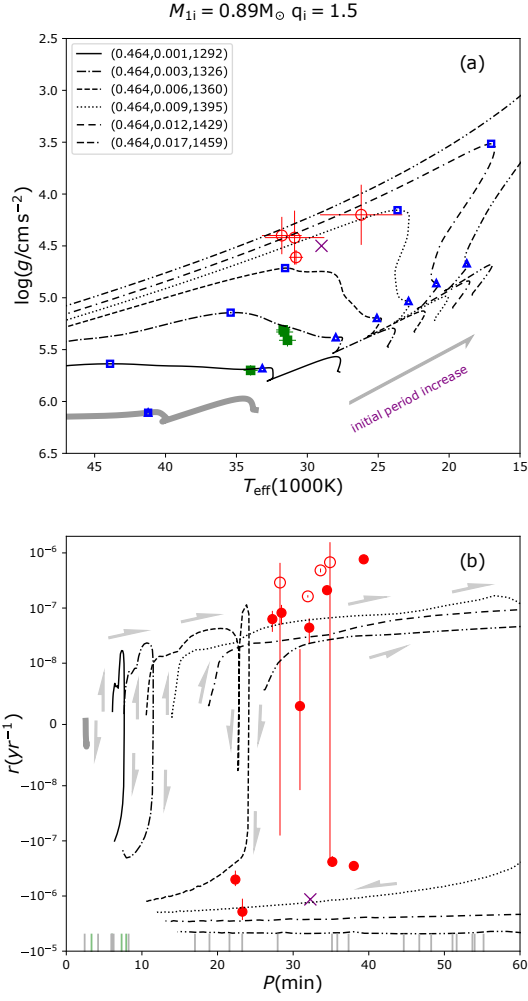


Fig. A.5. Evolution of sdBs produced by binaries, which is same as in Fig. 1, but for $(M_{1i}, q_i) = (0.89 M_{\odot}, 1.5)$.

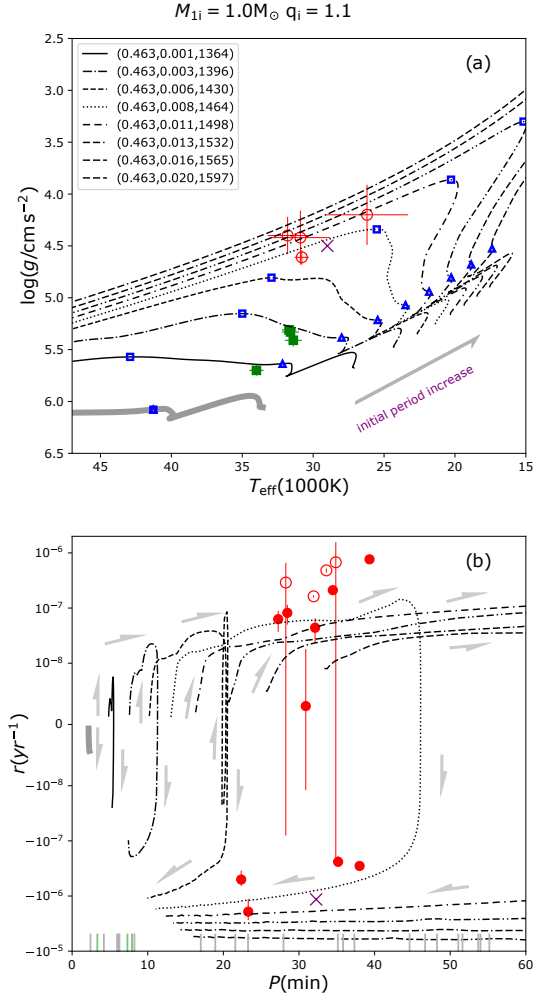


Fig. A.6. Evolution of sdBs produced by binaries, which is same as in Fig. 1, but for $(M_{1i}, q_i) = (1.0 M_{\odot}, 1.1)$.

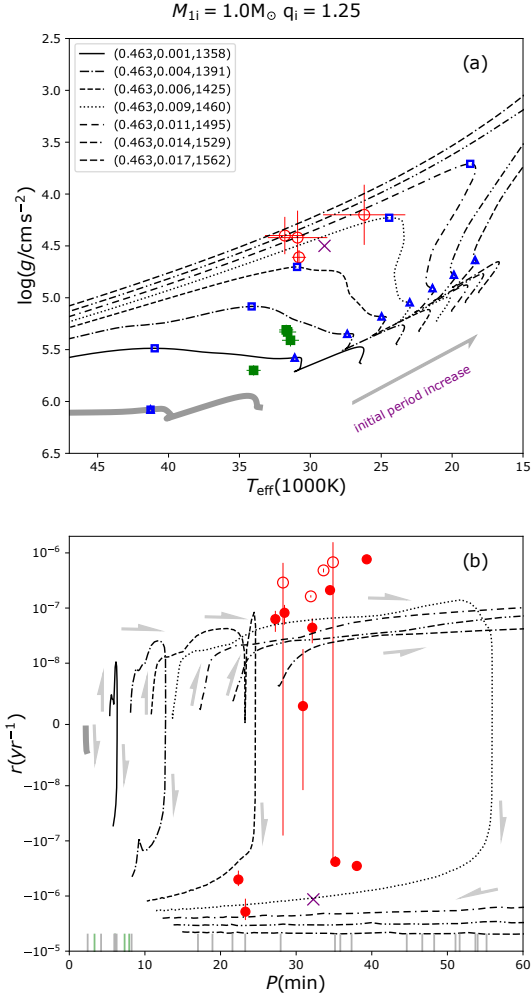


Fig. A.7. Evolution of sdBs produced by binaries, which is same as in Fig. 1, but for $(M_{1i}, q_i) = (1.0 M_{\odot}, 1.25)$.

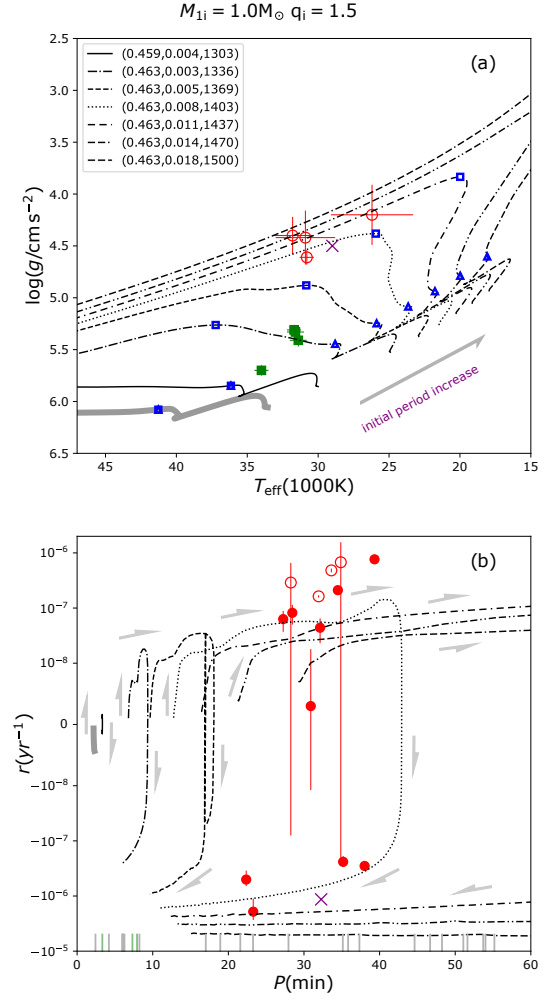


Fig. A.8. Evolution of sdBs produced by binaries, which is same as in Fig. 1, but for $(M_{1i}, q_i) = (1.0 M_{\odot}, 1.5)$.

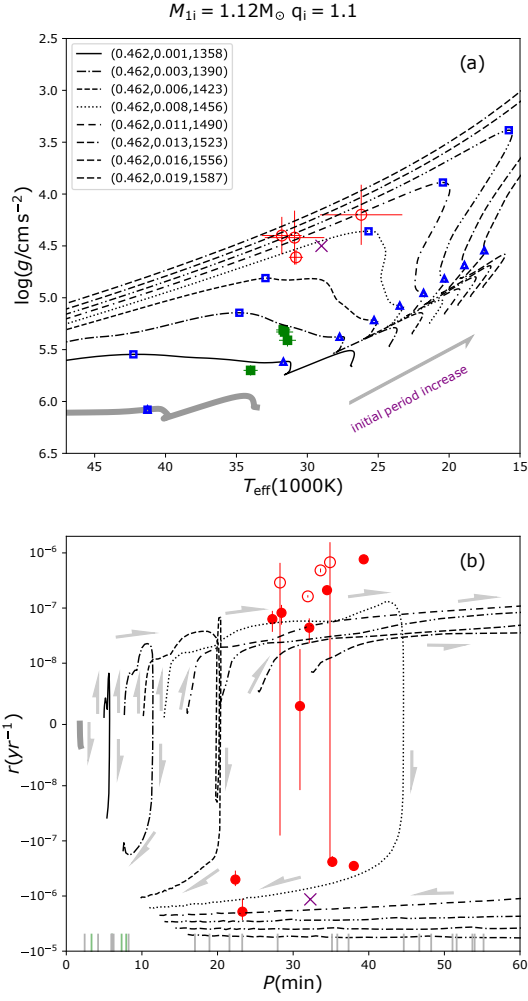


Fig. A.9. Evolution of sdBs produced by binaries, which is same as in Fig. 1, but for $(M_{1i}, q_i) = (1.12 M_{\odot}, 1.1)$.

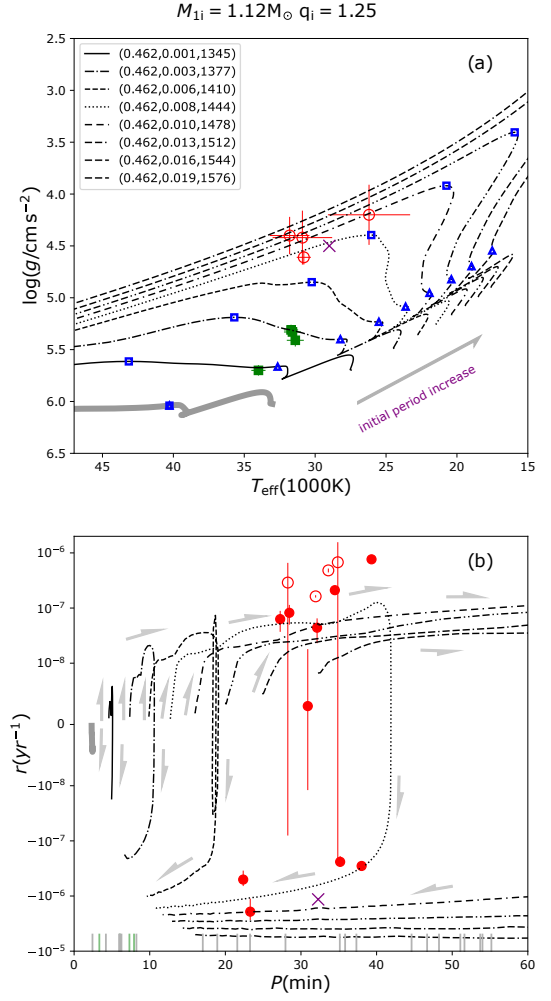


Fig. A.10. Evolution of sdBs produced by binaries, which is same as in Fig. 1, but for $(M_{1i}, q_i) = (1.12 M_{\odot}, 1.25)$.

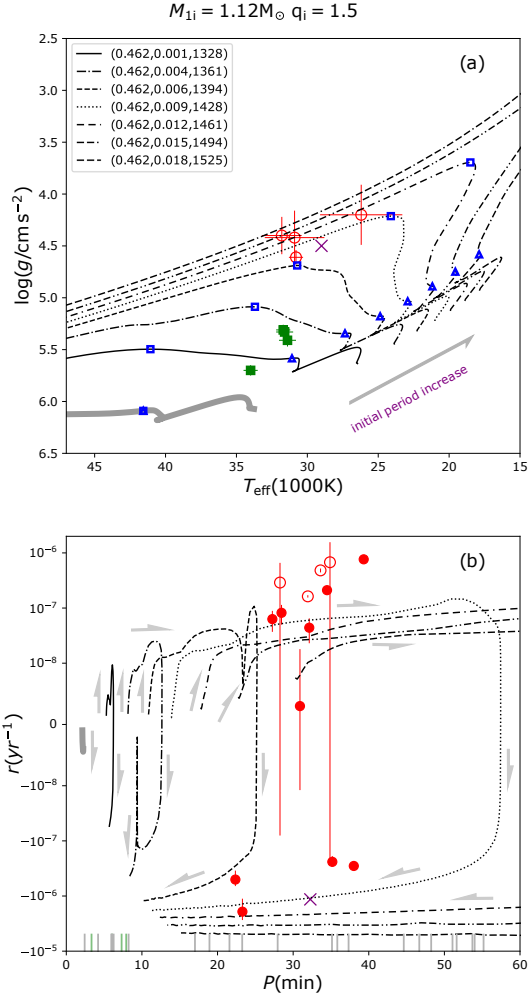


Fig. A.11. Evolution of sdBs produced by binaries, which is same as in Fig. 1, but for $(M_{1i}, q_i) = (1.12 M_{\odot}, 1.5)$.

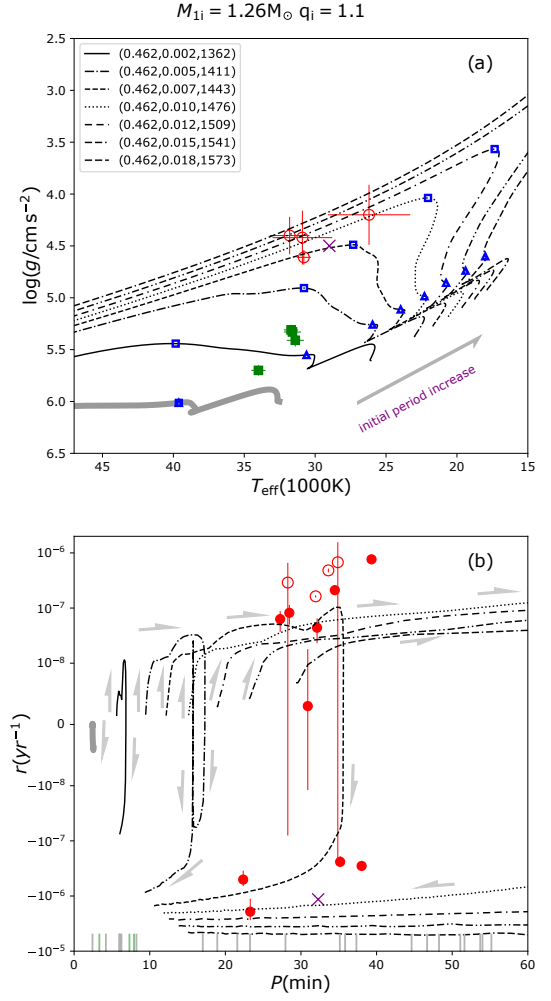


Fig. A.12. Evolution of sdBs produced by binaries, which is same as in Fig. 1, but for $(M_{1i}, q_i) = (1.26 M_{\odot}, 1.1)$.

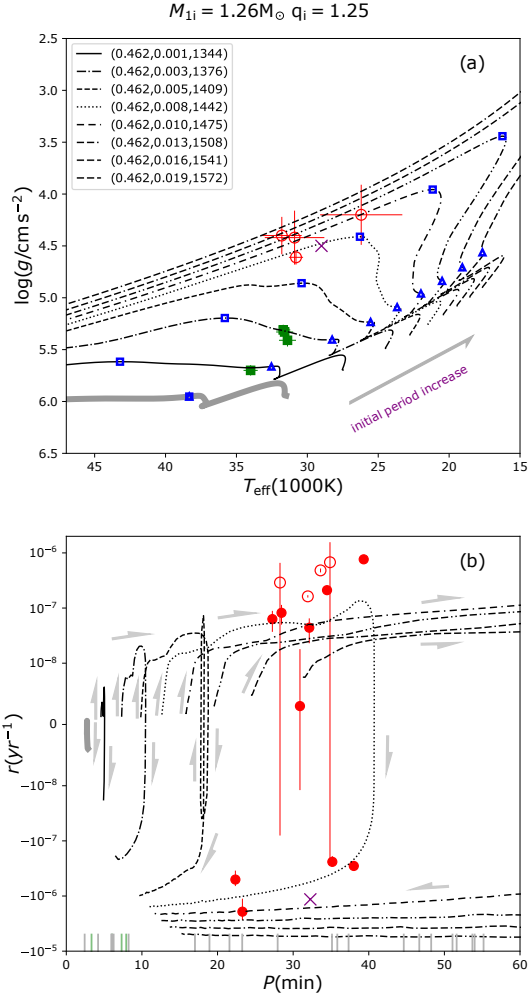


Fig. A.13. Evolution of sdBs produced by binaries, which is same as in Fig. 1, but for $(M_{1i}, q_i) = (1.26M_{\odot}, 1.25)$.

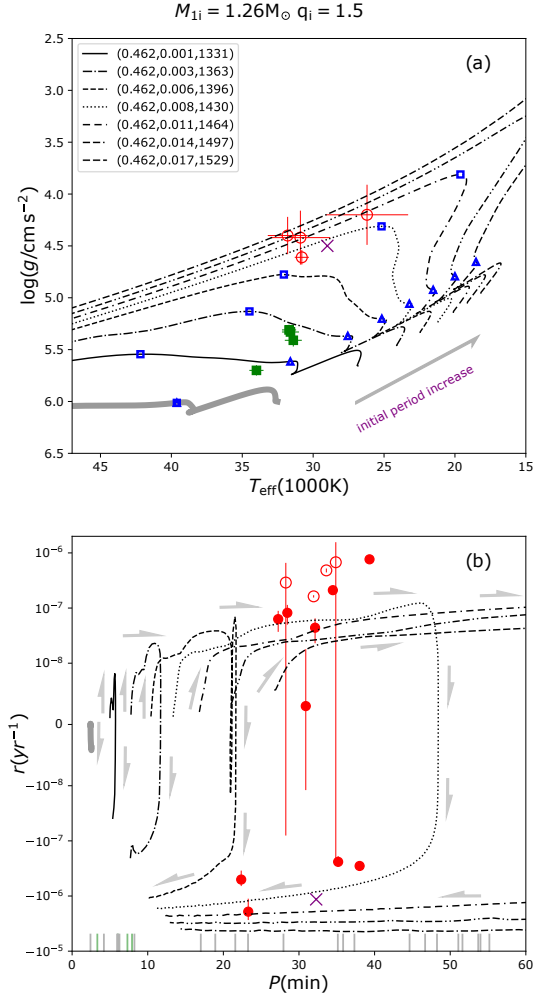


Fig. A.14. Evolution of sdBs produced by binaries, which is same as in Fig. 1, but for $(M_{1i}, q_i) = (1.26M_{\odot}, 1.5)$.

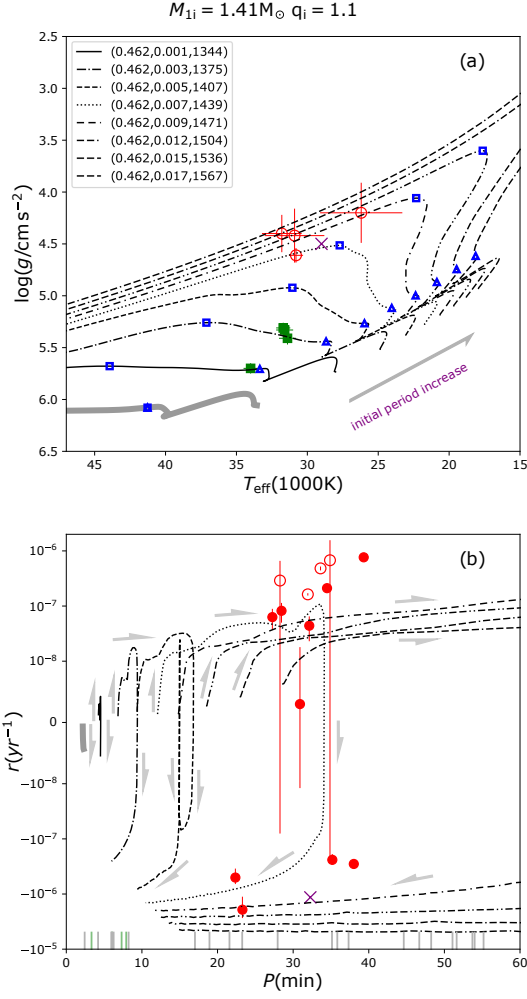


Fig. A.15. Evolution of sdBs produced by binaries, which is same as in Fig. 1, but for $(M_{1i}, q_i) = (1.41 M_{\odot}, 1.1)$.

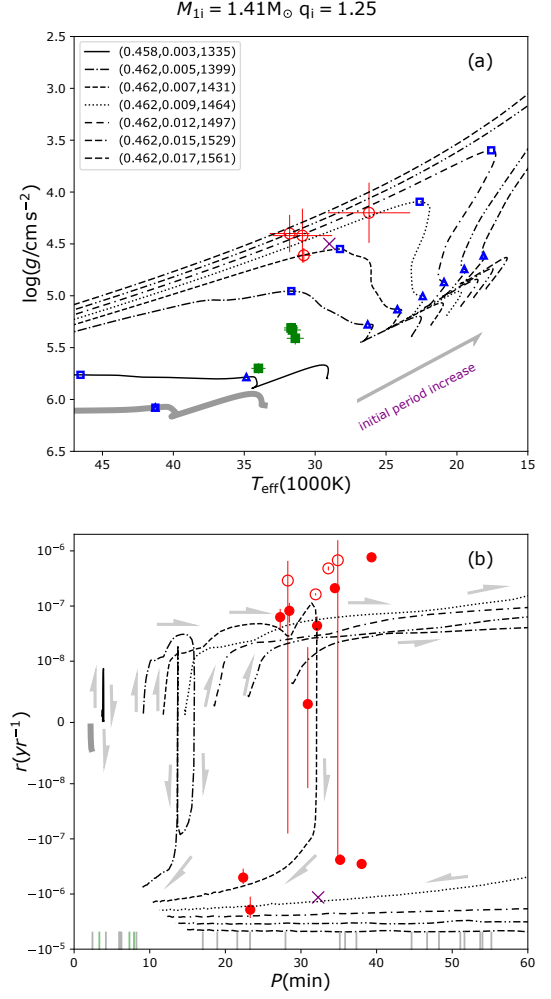


Fig. A.16. Evolution of sdBs produced by binaries, which is same as in Fig. 1, but for $(M_{1i}, q_i) = (1.41 M_{\odot}, 1.25)$.

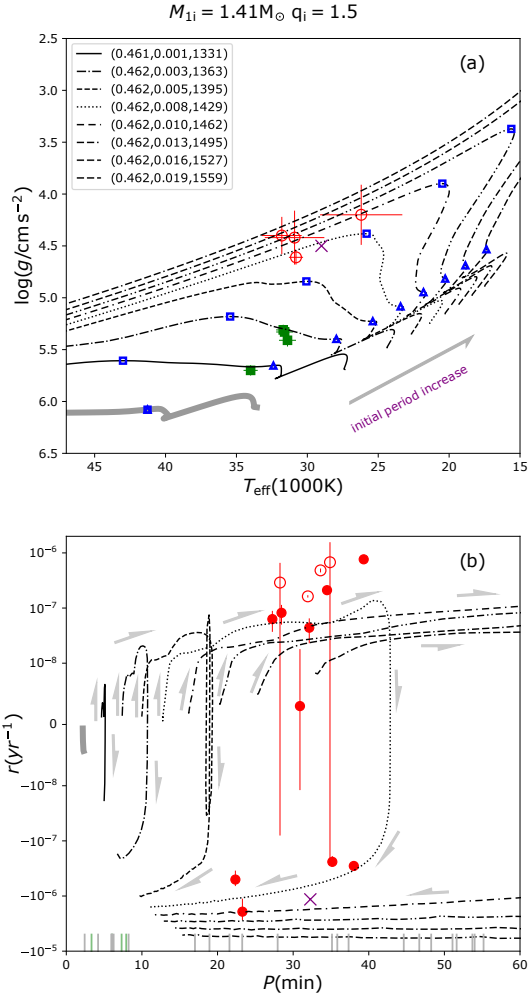


Fig. A.17. Evolution of sdBs produced by binaries, which is same as in Fig. 1, but for $(M_{1i}, q_i) = (1.41 M_{\odot}, 1.5)$.

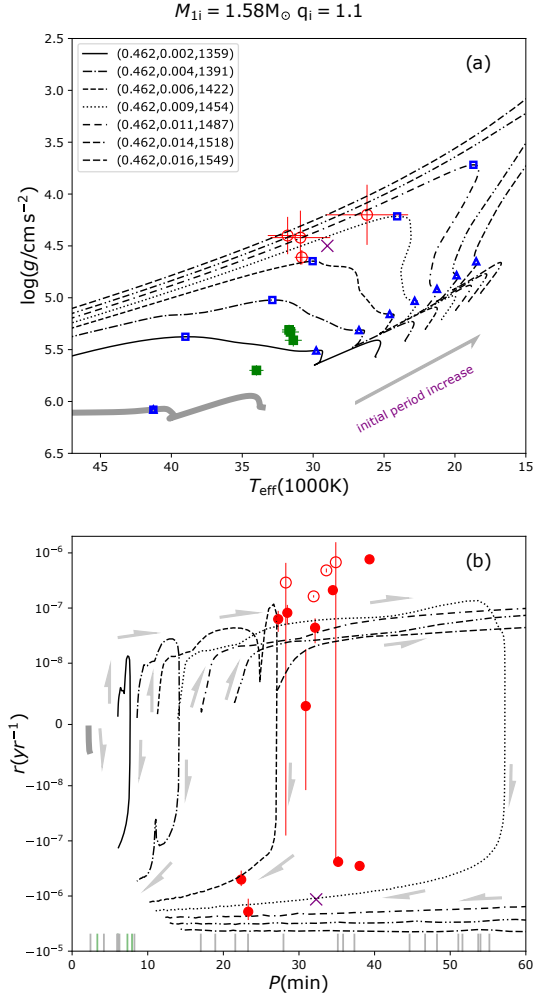


Fig. A.18. Evolution of sdBs produced by binaries, which is same as in Fig. 1, but for $(M_{1i}, q_i) = (1.58 M_{\odot}, 1.1)$.

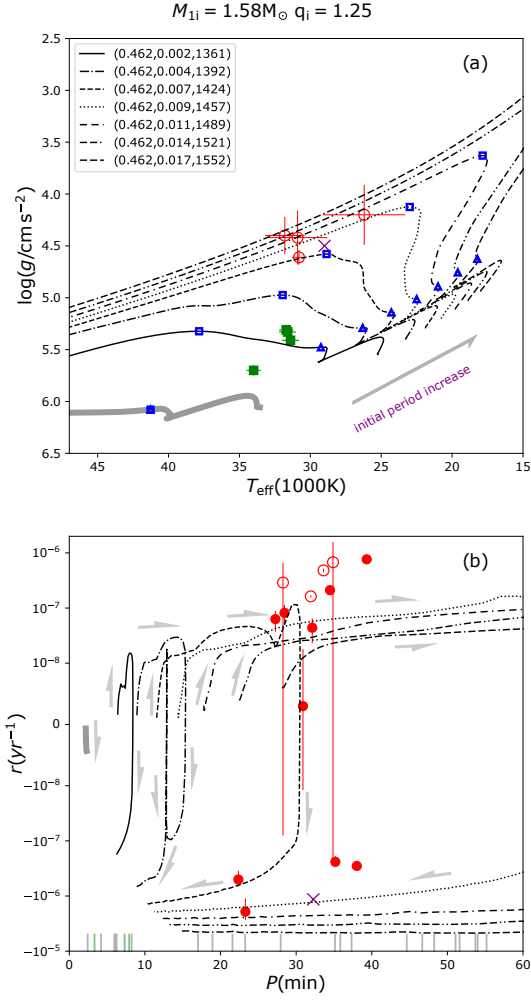


Fig. A.19. Evolution of sdBs produced by binaries, which is same to Fig. 1, but for $(M_{1i}, q_i) = (1.58 M_{\odot}, 1.25)$.

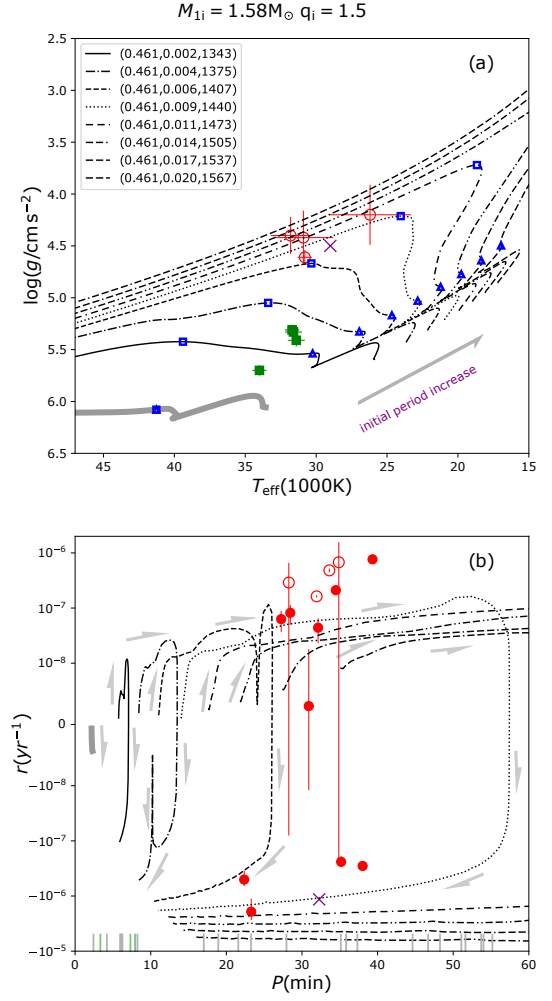


Fig. A.20. Evolution of sdBs produced by binaries, which is same as in Fig. 1, but for $(M_{1i}, q_i) = (1.58 M_{\odot}, 1.5)$.

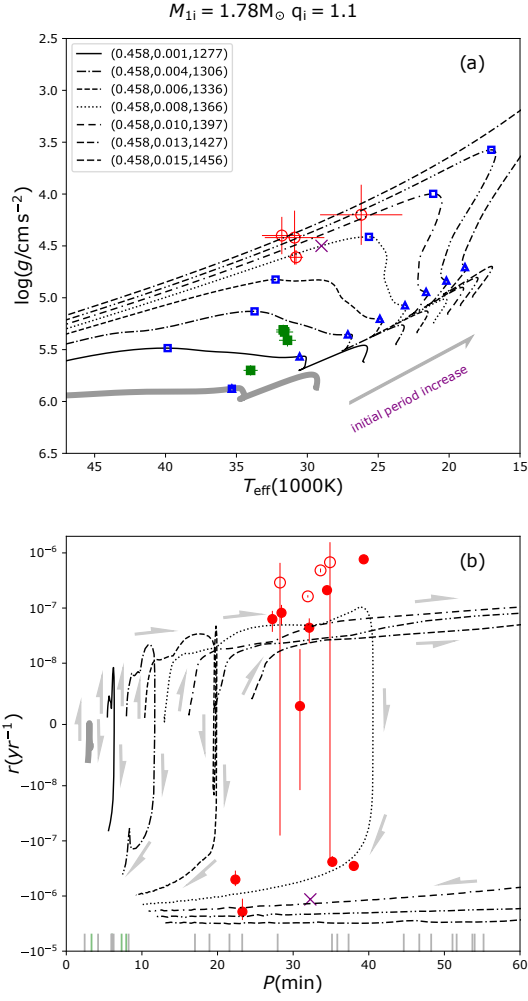


Fig. A.21. Evolution of sdBs produced by binaries, which is same to Fig. 1, but for $(M_{1i}, q_i) = (1.78 M_{\odot}, 1.1)$.

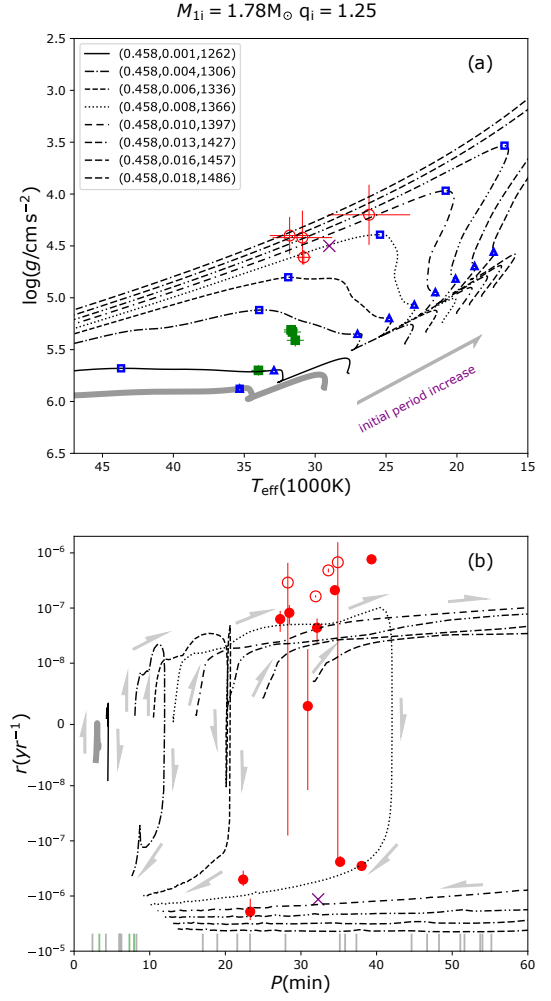


Fig. A.22. Evolution of sdBs produced by binaries, which is same as in Fig. 1, but for $(M_{1i}, q_i) = (1.78 M_{\odot}, 1.25)$.

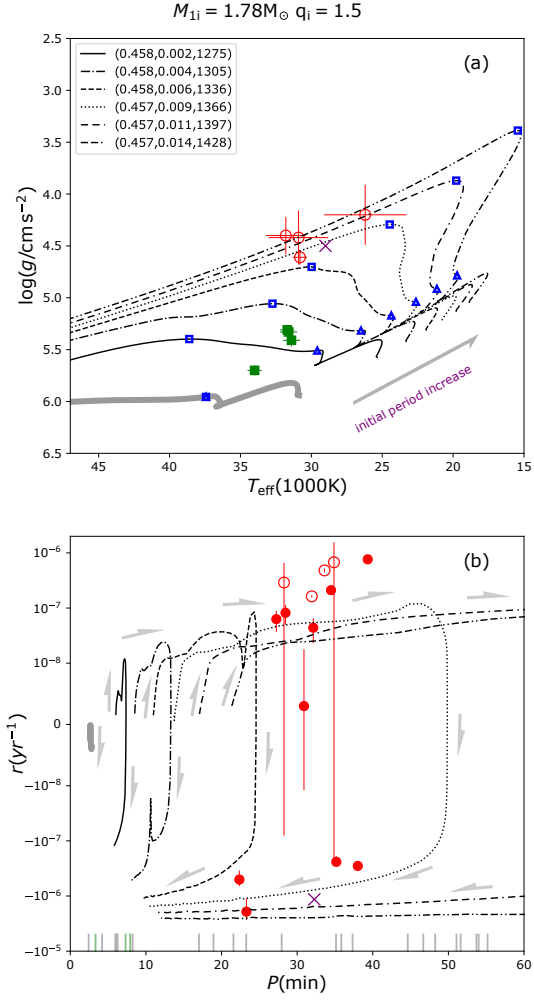


Fig. A.23. Evolution of sdBs produced by binaries, which is same as in Fig. 1, but for $(M_{1i}, q_i)=(1.78M_{\odot}, 1.19)$.